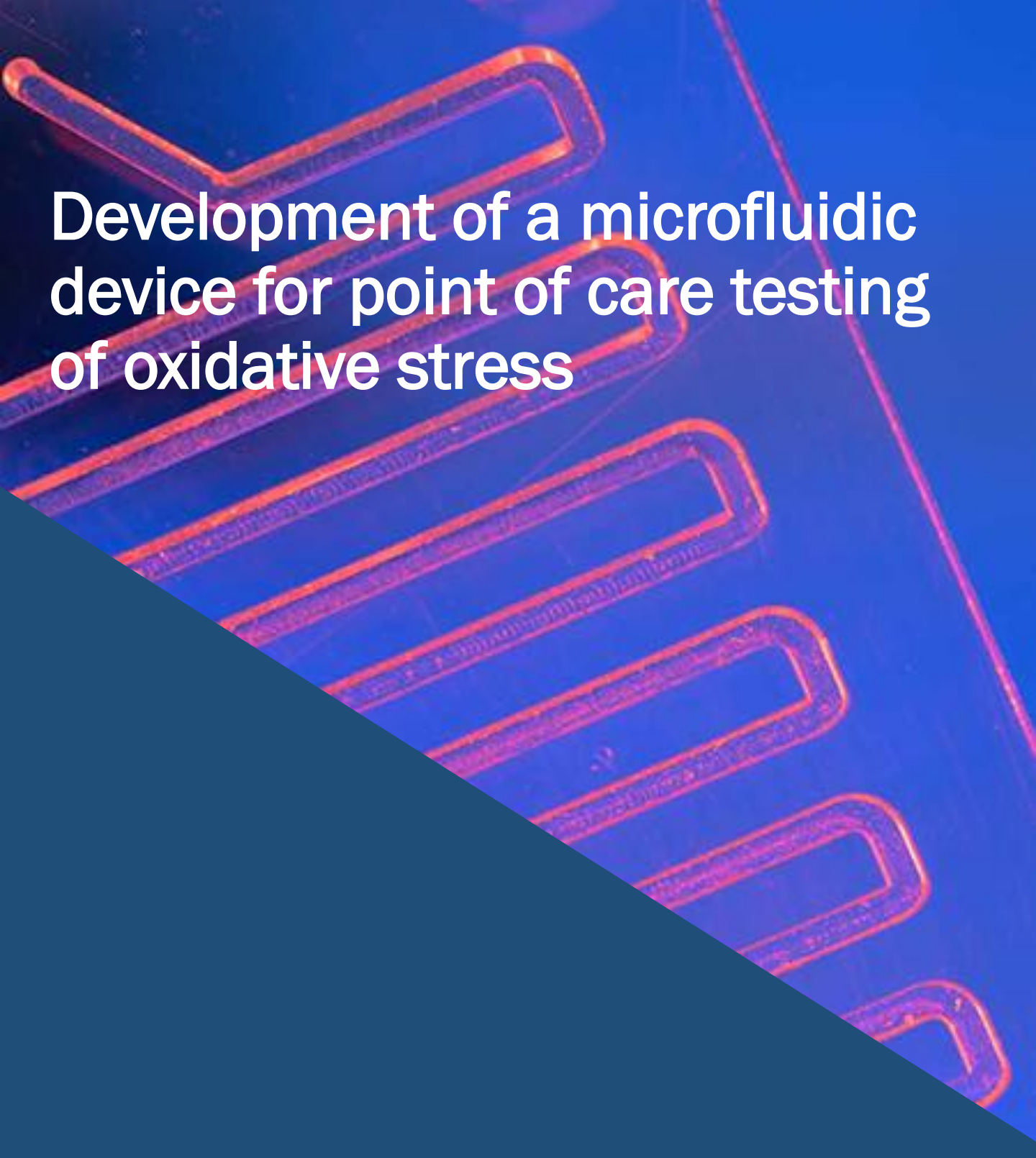

Development of a microfluidic device for point of care testing of oxidative stress

University of Twente &
University Medical
Center Groningen

Master Thesis - Esmay Hammink

Development of a microfluidic device for point of care testing of oxidative stress

Esmay Hammink

S1801406

July 2022

Supervisors

University of Twente

Prof. dr. ir. L.I. Segerink

Dr. ir. W. Olthuis

University Medical Centre Groningen

Prof. dr. H. van Goor

Drs. A.R. Bourgonje

Dr. S. J .Gordijn

Dr. A.C. Muller Kobold

Image front page adapted from Dr. Ruitao Su (University of Minnesota)

UNIVERSITY OF TWENTE.

GRC Groningen Redox Center

umcg

BIOS Lab on a Chip group

Abstract

Introduction: Oxidative stress, an imbalance between the generation of oxidants and the availability of anti-oxidants, is associated with multiple pathological conditions. Plasma free thiol levels reliably reflect the redox status, as the sulfhydryl group (R-SH) is readily oxidized by oxidants. Multiple studies have shown the potential of plasma free thiol levels as biomarker in various conditions, such as inflammatory bowel disease. Current detection of free thiols is time-consuming and laborious. In these thesis, first steps were taken towards the development of a microfluidic device for point-of-care detection of free thiols using finger-prick blood.

Materials & Methods: The standard protocol for free thiol detection with 5,5-dithio-bis-2[2-nitrobenzoic acid] (DTNB) described by Ellman was adjusted and applied to lower plasma samples. A polymethylmethacrylate (PMMA) master mould was fabricated using micro milling for the replication of polydimethylsiloxane (PDMS) microfluidic devices, in which absorbance measurements were performed. Trigger valves with different geometries were designed and tested. These trigger valves were combined with passive micromixer structures to enable on-chip mixing of DTNB and diluted plasma.

Results: Free thiol measurements of 6 μL plasma resulted in an average inter-coefficient of variation (CV) below 5% and an intra-CV below 11% (n=8). On-chip absorbance measurements resulted in an intra-CV below 4% (n=6). The determined concentrations were comparable to the values obtained with the standard protocol. Trigger valves were able to temporarily stop (at least 10 minutes) fluid flow using a pressure barrier. The current design of the mixing component does not noticeably increase mixing efficiency and needs optimization.

Conclusion: Our results show the promising potential of microfluidic devices for the rapid determination of free thiols in small volume plasma samples. To achieve point-of-care testing, further sample preparation steps need to be integrated on the microfluidic device such as plasma separation and dilution.

Samenvatting

Introductie: Oxidatieve stress, een disbalans tussen de generatie van oxidanten en de beschikbaarheid van anti-oxidanten, wordt geassocieerd met verscheidene pathologische condities. Plasma vrij thiolen levels weerspiegel betrouwbaar de redox status, aangezien de sulfhydryl groep (R-SH) gemakkelijk geoxideerd wordt door oxidanten. Meerdere onderzoeken hebben de potentie van plasma vrije thiolen levels laten zien als biomarker in verschillende ziektebeelden, zoals bijvoorbeeld inflammatory bowel disease. De huidige detectie van vrije thiolen is tijdrovend en arbeidsintensief. In deze thesis zijn de eerste stappen gezet voor het ontwikkelen van een microfluidic device voor het point-of-care detecteren van vrije thiolen in vingerprik bloed.
Materialen & Methodes: Het standaard protocol voor het detecteren van vrije thiolen met gebruik van 5,5-dithio-bis-2[2-nitrobenzoic acid] (DTNB) beschreven door Ellman is aangepast en toegepast op lagere plasma volumes. Een polymethylmethacrylaat (PMMA) master mould is gefabriceerd door middel van micro millen voor de replicatie van polydimethylsiloxaan (PDMS) microfluidic devices, waarin absorptie metingen zijn uitgevoerd. Trigger valves met verschillende afmetingen zijn ontworpen en getest. Deze trigger valves zijn gecombineerd met een passieve micromixer structuren voor het on-chip mixen van DTNB en verdund plasma.
Resultaten: Vrij thiol metingen in 6 μL plasma resulteerden in een gemiddelde inter-coefficient of variation (CV) lager dan 5% en een intra-CV lager dan 11% (n=8). On-chip absorptie metingen resulteerden in een intra-CV lager dan 4% (n=6). De bepaalde concentraties waren vergelijkbaar met de waardes verkregen met het standaard protocol. Trigger valves waren in staat om de vloeistof flow tijdelijk te stoppen (tenminste 10 minuten). Het huidige ontwerp van de mixer verhoogt niet zichtbaar de mixing efficiency en vraagt om verdere optimizatie.
Conclusie: De resultaten tonen het veelbelovende potentieel van microfluidic devices n voor de snelle bepaling van vrije thiolen in plasma samples met een klein volume. Om point-of-care-testen te bereiken moeten de andere stappen van het protocol geïntegreerd worden, zoals plasma scheiding en verdunning.

List of Abbreviations

AgNPs	Silver Nanoparticles
AuNPs	Gold Nanoparticles
CV	Coefficient of Variation
DTNB	5,5'-dithio-bis-2[2-nitrobenzoic acid]
HMW	High Molecular Weight
IBD	Inflammatory Bowel Disease
LDR	Light Dependent Resistor
LED	Light Emitting Diode
LOC	Lab-on-a-Chip
LoD	Limit of Detection
LoQ	Limit of Quantification
LMW	Low Molecular Weight
PDMS	Polydimethylsiloxane
PMMA	Polymethylmethacrylate
POC	Point-of-Care
POCT	Point-of-Care Testing
PQQ	Pyrroloquinoline quinone
RNS	Reactive Nitrogen Species
ROS	Reactive Oxygen Species
SD	Standard Deviation
SE	Standard Error
TNB	2-nitro-5-thiobenzoic acid
UMCG	University Medical Center Groningen

Contents

1 Introduction

This master thesis is part of a project which is a collaboration between the University Medical Center Groningen (UMCG) and the BIOS Lab on a Chip group from the University of Twente. From the UMCG, people from different specialisations are involved: Pathology, Gynaecology, Gastroenterology and Hepatology and Clinical Chemistry.

Oxidative stress, an imbalance between oxidants and anti-oxidants, is a process extensively studied in literature. Oxidative stress is proven to play a key role in a variety of diseases, e.g. inflammatory bowel disease, cardiovascular disease, brain disorders and placental dysfunction. Currently it is not technically possible to reliably quantify levels of oxidative stress at point-of-care. Therefore, the ultimate goal of this collaboration is to develop a microfluidic device for point-of-care testing of oxidative stress. During this thesis, first steps were taken towards the design and fabrication of a microfluidic device for point-of-care testing of oxidative stress.

The work performed during this project was presented with an oral presentation at the International Conference on Oxidative Stress Reduction, Redox Homeostasis & Antioxidants (22-24 June 2022, Paris, France). The submitted abstract to this conference can be found in appendix A.

2 Background

2.1 Oxidative Stress

The redox status can be described as the balance between oxidants and anti-oxidants. [1] Oxidants, such as reactive oxygen species (ROS), are continuously produced in the cell. The term ROS refers to oxygen-centered free radicals and non-radical but reactive derivatives of oxygen. They are chemically reactive molecules, which are necessary for multiple physiological processes such as intracellular cell signalling, homeostasis, cell death and the immune defence against pathogens. [2] They are produced by different pathways and released from several cell types. For example, phagocytes produce and release ROS to neutralize invading particles. ROS are also a secondary messenger in some major pathways of cell signalling, allowing the transduction of extracellular stimuli into changes in cell physiology. [3] ROS is thus of importance in the body. However, if they are present in excessive amounts this can result in damage to DNA, proteins, lipids and nucleic acids, possibly leading to cell death or tissue destruction. To prevent excessive levels of ROS, the human body is equipped with an anti-oxidant system to regulate the levels of these reactive species. [2] Anti-oxidants are any species that delay, prevent or remove oxidants from causing damage. The most important ones are considered to be urate, abundant proteins such as albumin and ascorbate. [4] When an imbalance between the generation of oxidants and the availability of anti-oxidants leads to an excess in oxidants, we speak of oxidative stress. As mentioned before, this excess in oxidants leads to oxidative damage; biomolecular damage caused by the modification by ROS. [5]

More and more studies are being published showing that an increase in oxidative stress can be associated with multiple pathological conditions. An increase in ROS production has been described in multiple cardiac conditions such as myocardial fibrosis, metabolic syndrome, cardiac hypertrophy, heart failure and myocardial infarction. [6] Oxidative stress also plays a role in the pathogenesis and progression of inflammatory bowel disease (IBD). [7] Furthermore, chronic inflammatory diseases such as asthma, chronic obstructive pulmonary disease, psoriasis and rheumatoid arthritis show increased oxidative stress at the site of inflammation. Neurodegenerative diseases such as Alzheimer's, Parkinson and amyotrophic lateral sclerosis are also associated with an increase in oxidative stress. [3] An increase in oxidative stress may also predict pregnancy complications, such as placental ischemia and preeclampsia. [8] This shows that oxidative stress could be an interesting biomarker for the diagnosis and monitoring of various conditions.

2.2 Biomarkers of Oxidative Stress

A biomarker can be defined as a substance, structure or process that can be measured in the body and influences or predicts the incidence, outcome or progression of disease. [9] Various biomarkers of oxidative stress can be measured.

Direct measurement of oxidants would be the ideal method if it could be reliably measured. However, ROS and reactive nitrogen species (RNS) are highly reactive and thus unstable compounds with a short lifetime. [3] This makes direct measurement of oxidants not reliable, therefore other biomarkers of oxidative stress should be explored. [10]

Indirect measurement of oxidative damage is an alternative approach, where damage of biomolecules that is caused by oxidants is quantified. By-products of ROS activity on biomolecules, such as breakdown products of cell membranes, can be detected. These methods have their limitations, as these break-down products are not specific for oxidative stress. They can also be produced as the result of other processes. Protein and lipid damage can also be detected, however the intensity of the oxidative stress measured indirectly is dependent on the type of oxidants released, as each biomolecule is affected by another type of oxidant. Furthermore, measuring a single type of molecule does not give a complete image of the total oxidative stress status. [3]

The anti-oxidant status displays the capacity to inhibit the transformation of a substrate by oxidants. [3] As oxidative stress is an imbalance between the oxidant and anti-oxidant state, measuring a decrease in the availability of anti-oxidants could be correlated to the extent of oxidative stress. [2] The extracellular fraction of free thiols could be viewed as a systemic redox buffer, as they are common targets of oxidants. Therefore, the level of extracellular free thiols is a reliable reflection of the redox status as they display the anti-oxidant availability. [11] This makes them an interesting biomarker, as reduced free thiol serum levels when compared with other oxidative stress biomarkers more accurately reflect the systemic redox status. [12]

2.3 Free Thiols

Free thiols are an important target molecule for oxidants due to their nucleophilicity and reactivity. [13] A thiol is a compound carrying a sulfhydryl (R-SH) group; a sulphur atom and a hydrogen atom attached to a carbon atom. In the human blood, thiols are present as both low- and high molecular weight thiols. The low molecular weight (LMW) thiols are mainly composed of glutathione, cysteine and homocysteine, which are thiol-containing amino acids. The high molecular weight (HMW) thiols are protein thiols, of which albumin is the most abundant. Free thiols can undergo an oxidation reaction with oxidants and form disulphide bonds (Fig. 1). Therefore, thiols can be present in the reduced (free) or oxidized (bound) state. Oxidized thiols are bound to another thiol via a disulfide bridge. This can be between two equal thiols (symmetric disulfides) or two different LMW thiols or a LMW thiol and a protein (mixed or asymmetric thiols). [12]

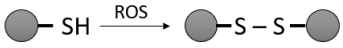

Figure 1: Oxidation of a free thiol to a disulfide bridge.

Compared to the intracellular compartment, plasma free thiols are considerably more oxidized and present at much lower concentrations. In plasma, the average total free thiol level is between 400 and 600 μM. The LMW thiols account for only 12-20 μM, the most abundant part is accounted for by protein thiols. Albumin is the most abundant protein thiol in plasma (600 μM), which is mostly present in the reduced form (75%). [13] Table 1 shows an overview of the most abundant compounds contributing to thiol levels in plasma. Albumin consists of 17 disulfide bonds and one free cysteine (Cys34), of which about 75% is reduced. [14] This makes Cys34, and therefore albumin, the most important anti-oxidant scavenger in plasma; it contributes to 80% of the anti-oxidant capacity. [15]

Table 1: Thiol levels in plasma. [13]

Species	**Concentration (μM)**
Total Albumin	527-783
Reduced	422 ± 52
Total Cysteine	202-281
Reduced	8.3-10.7
Total Homocysteine	6.5-11.9
Reduced	0.17-0.32
Total Glutathione	4.9-7.3
Reduced	2.0-5.1

.

2.3.1 Free Thiols as Biomarker

Many studies have focused on the relation between serum/plasma free thiol levels and disease activity. Bourgonje et al. [16] concluded that serum free thiols are reduced in patients with IBD and are superior to the golden standard (fecal calprotectin levels) when discriminating between disease activity. Abdulle et al. [17] shows that serum free thiols predict the risk of cardiovascular events and all-cause mortality. Schoots et al. [18] showed that pregnant women with severe fetal growth restriction (FGR) and preeclampsia (PE) showed significantly reduced free thiol levels in plasma. Relations have also been proven in e.g. renal failure [19], type 2 diabetes mellitus [20] and neurodegenerative diseases such as Alzheimer's and Parkinson [21]. These examples show the potential of free thiols in serum and/or plasma as a biomarker for numerous diseases. Free thiols are not only a promising biomarker for diagnosis, but also for monitoring of disease progression, risk assessment and response to treatment.

2.4 Point-of-care Testing

The overcrowding of the hospital, in particular at the emergency department, is a major current problem in the health care system. Overcrowding is associated with an increase in patient mortality and also negatively affects other health care in the hospital. [22] Point-of-care testing (POCT) could help address this problem. A point-of-care (POC) test is a simple test that can rapidly

provide diagnostic results near the patient. POCT enables more rapid clinical decision making in the process of diagnosis, monitoring and therapy. [23] In addition to enabling rapid testing and decision making, POCT could reduce the amount of hospital visits by enabling testing at the general practitioner or even at home. [22] Furthermore, as POCT requires smaller sample volumes than regular clinical tests, there is less discomfort for the patient. [24]

As stated before, oxidative stress plays a key role in multiple conditions. Therefore it could be interesting for many applications to be able to rapidly determine the level of plasma free thiols near the patient. For example, enabling at-home monitoring of IBD progression could decrease the number of required hospital visits. However, POC determination of free thiol levels is not yet possible. Current determination of free thiol levels requires the referral of a sample to a specialized central laboratory. Besides the detection being time-consuming and laborious, the sample can also degrade leading to ambiguous results.

2.5 Microfluidics

Microfluidic technologies are often applied for the development of POC diagnostics. Microfluidic devices, also often called lab-on-a-chip (LOC) systems, are instruments that use small amounts of fluids on a microchip to perform laboratory tests. [25] A LOC is a device that integrates several analytical functions on a small single device. Processes which are normally performed in a laboratory by trained personnel can be miniaturized on a single chip. [26] An ideal microfluidic device for POCT is a 'sample-in-answer-out' system, meaning that all sample preparation steps and analysis are automatically performed on a single device. [23] Microfluidic devices offer many advantages such as smaller sample volumes, low cost, reduction of human error, faster response time and diagnosis, robustness, high sensitivity and fast turn-around times. It is possible to incorporate the detection of multiple analytes in one sample, make them user-friendly and equipment-free. [25]

3 Aim of Thesis

The aim of this project is to develop a microfluidic device to enable POCT of oxidative stress, by measuring free thiol levels in human plasma.

3.1 Requirements device

To obtain POCT and ensure optimal translation from research to clinical setting, the following requirements are set-out for the microfluidic device:

- Affordable.
- User-friendly; easy to use with minimal training.
- Rapid read-out; for our device, we aim at a read-out within 30 minutes.
- Robust.
- No need for bulky external equipment.
- Deliverable; available for end-users.
- Easily obtainable, low volume sample; whole finger-prick blood.
- Detection range of 200-800 μM free thiols in plasma (as the physiological range is 400-600 μM).
- Sufficient (analytical) sensitivity; the smallest amount of substance in a sample that can accurately be measured by an assay. The maximum allowed Limit of Detection (LoD) is set at 100 μM.
- Sufficient (analytical) specificity; the ability of a device to measure a particular substance, rather than others, in a sample. The device should have no interference of other compounds present in the sample.
- Quantitative read-out.
- Monolithic approach; all steps are performed on one device.

4 Literature Research: Detection Methods of Free Thiols

4.1 Detection Principles of Microfluidic Devices

Various detection principles can be used for the detection of biomarkers in microfluidic devices. They all have their own disadvantages and advantages, depending on the application. The three major types of microfluidic detection principles are 1) optical detection 2) electrochemical detection and 3) mass-sensitive detection. [27] Optical and electrochemical methods are most frequently utilized due to their selectivity and sensitivity. [28]

Electrochemical detection can be divided into amperometry, potentiometry and conductometry measurements. [28] The most frequently used biosensors are based on amperometry; a current is generated in proportion to the concentration of the detected analyte. Potentiometry relies on measuring a potential difference between two reference electrodes. Conductometry detects a change in impedance, caused by a change in resistance. [27] Electrochemical detection is attractive for microfluidic applications due to the versatility of size, geometry and nature of electrodes and its easy integration. Furthermore, they have a fast response, high sensitivity, accuracy, low LoD, good scalability and are low in cost. In contrast to optical detection, miniaturization generally enhances the sensitivity and LoD of the measurement. [29]

Optical detection can be divided into two groups, depending on the property of light that is detected. The most straightforward group relies on measuring a direct change in the light intensity e.g. for absorbance, fluorescence or chemiluminescence detection. The more sensitive group relies on inducing a change in the wavelength, phase or polarization in the light. [28] Absorbance measurements are based on changes in optical density. With fluorescence, the intensity of the emitted light is detected. [29] Optical detection can be off-chip; in which detection components are not integrated within the microfluidic device, or they can be integrated in the devices (on-chip). [30] Optical detection is popular due to easy incorporation of microfluidic devices into conventional optical devices, as no interconnection is required between the detector unit and the microfluidic device. Another advantage of optical detection is that only photons are involved in optical detection, thus minimal disturbance is caused to the sample matrix. The key challenge with optical detection in microfluidics is the short path length of microchannels, especially when performing absorbance measurements. [31]

4.2 Electrochemical Detection of Free Thiols

As mentioned above, electrochemical detection is an attractive detection method to integrate in microfluidic devices, due to its great scalability. However, electrochemical detection of thiols is a challenge due to their poor voltammetric behaviour at solid electrodes. To acquire sufficient sensitivity (low LoD), large overpotentials are required. This high potential can result in responses from other oxidisable species present in the sample, compromising the analytical specificity. Human plasma contains many species that may be redox active or interfere with the measurement. [32] Furthermore, passivation of the electrode surface occurs. [33] Multiple studies have been performed studying solutions to avoid the need of large overpotentials and thus enable the detection of free thiols in complex biological solutions.

Various studies use **electrocatalysts**, either immobilised on the electrode surface or added to the sample, to lower the potential. Gracheva et al. [34] utilizes quinone naphthoquinone to react selectively with free thiol groups in plasma, which results in a drop in electrode potential. The selective nucleophilic addition of thiols to the quinone indicator results in the production of quinone-thiol conjugates. This alters the redox balance, which can be detected at a screen-printed electrode assembly. However, electrode fouling is still an issue and a high dilution of the sample is utilized in the study (50 μL plasma to 10 mL buffer), resulting in high sample volumes. Inoue et al. [35] incorporates the coenzyme pyrroloquinoline quinone (PQQ) into the electrode to lower the required potential. However, PQQ is reported to be involved in many enzymatic reactions and could therefore also react with other nucleophilic substances found in plasma. Ascorbic acid and uric acid, both normally present in plasma, were proven to interfere with the detection method. Lawrence et al. [33] utilized catechol as an electrochemical indicator for the detection of thiols, however experiments were only performed in culture media and not in human plasma or serum.

Electrochemical detection can also be combined with a **separation method**, such as chromatography, to reduce the interference of the other species present in plasma. Chromatography combined with electrochemical detection is often used for the determination of electroactive compounds in mixtures. However, this adds an extra step to the microfluidic device and is therefore not ideal. [36]

Other studies utilize **mercury-based electrodes**. Thiols interact with these electrodes to form stable mercury-thiolate complexes. After a given deposition period, a negative electrode potential is used to reduce metal ions to metal. The resulting peak current can be correlated to free thiol levels. This technique enables detection at a less positive potential. [32] However, this approach requires an initial separation method to be able to determine thiol levels in complex biological samples. [35]

4.3 Optical detection of free thiols

Absorbance measurements are easy, quick, cost-effective and straightforward. The challenge lies with obtaining sufficient sensitivity and low LoD, as a decrease in path length lowers the sensitivity. For the absorbance measurements of free thiols, DTNB (Ellman's reagent) is frequently utilized. DTNB reacts with free thiols and forms 2-nitro-5-thiobenzoic acid (TNB), which is a measurable yellow-colored product with a maximum absorption at 412 nm. [37] No microfluidic devices have been developed which utilize Ellman's reagent to detect free thiols in plasma. However, Supharoek et al. [38] fabricated a polydimethylsiloxane (PDMS) chip with a light emitting diode (LED) as light source and light dependent resistor (LDR) as light sensor. The concentration of glutathione in dietary supplement samples was successfully determined after the reaction with DTNB. Researchers at the UMCG also utilize DTNB for the detection of free thiols in serum and plasma samples. 20 μL of 1.9 mM DTNB is added to 90 μL 1:4 diluted serum in a 96 wells plate, after which absorbance measurements are performed.

Indirect detection of free thiols is also possible with absorbance measurement, e.g. with the use of nanoparticles. Ghasemi et al. [39] makes use of the fact that free thiols show a strong affinity with noble metal nanostructures (e.g. gold/silver). Gold Nanoparticles (AuNPs) are plasmonic nanomaterials; they have shape and size-dependent optical properties. Free thiols bind to the surface of these AuNPs and induce aggregation, thereby changing their colour. However, this technique is not suitable for HMW thiols, as steric hindrance decreases interaction between HMW thiols and the AuNPs. Xu et al. [40] utilizes the fact that Hg^{2+} ions induce aggregation of AuNPs. Biothiols bind to Hg2+ and therefore prevent the aggregation of AuNPs. However, Hg^{2+} also binds to disulfide bridges in albumin, this method is therefore only suitable for LMW thiols.

Fluorescence-based biosensors make use of fluorescent probes that directly or indirectly measure the free thiol content. Fluorescence-based sensors are often highly sensitive with a low LoD. Current research is performed to fabricate tools to enable POC fluorescence measurements. [41] Multiple studies have been performed exploring fluorescent probes for the detection of thiols, both with a direct and indirect approach. However, only few studies focus on the detection of HMW thiols next to LMW thiols. Sun et al. [42] utilizes a fluorescent Naph-EA-mal probe, with a maleimide as a thiol acceptor. The probe shows high selectivity and fast response toward thiols in aqueous solutions. Hu et al. [43] utilized carbonaceous nanospheres loaded with silver nanoparticles (AgNPs) as carriers. Reporter dyes are attached to the surface of AgNPs, due to a place-exchange process with free thiols the reporter dyes are released into the solution, which increasing fluorescence intensity can be measured and correlated to free thiol concentration.

Table 2: Summary of electrochemical detection methods of free thiols.

Technique	**Matrix**	**Analyte**	**LoD & Linear range**
Electrocatalyst; naphthoquinone, potentiometric detection [34]	Human plasma	Total free thiols	0.4 μM (0.4-100 μM)
Electrocatalyst; pyrroloquinoline quinone, amperometric detection [35]	Borate buffer & Dietary supplement	Cysteine Homocysteine N-acetylcysteine Glutathione	63.7 nM 447 nM 2.62 nM 1.32 nM
Electrocatalyst; catechol, potentiometric detection [33]	Culture media	Cysteine Glutatione Homocysteine	6 μM (12-50 μM) 7 μM (6-59 uM) 1 μM (11-53 μM)
Liquid Chromatography coupled to amperometry [36]	Buffer	Cysteine Glutathione Dithiothreitol Albumin	3.8 μM (10-100 μM) 3.9 μM (10-100 μM) 3.4 μM (5-50 μM)

Table 3: Summary of optical detection methods of free thiols.

Technique	**Matrix**	**Analyte**	**LoD & Linear Range**
Absorbance: DTNB on-chip [38]	Dietary supplement	Glutathione	32 nM
Absorbance: gold nanoparticle aggregation [39]	Human plasma	Cysteine Glutatione	0.5 μM 10 μM (200-800 μM)
Absorbance; Hg2+ mediated gold nanoparticle aggregation [40]	Urine	Glutathione Cysteine Homocysteine	17 nM(0.025-2.28 μM) 9 nM (0.035-1.53 μM) 18 nM (0.040-2.20 μM)
Fluorescence: Naph-EA-mal probe [42]	Tris-HCL, Lysed cells Fixed cells	Albumin Cysteine Homocysteine Glutathione	– 2.21 nM 3.31 nM 3.54 nM
Fluorescence; nanospheres loaded with silver nanoparticles carrying reporter dyes [43]	Sodium acetate buffer	Cysteine Glutathione Bovine Serum Albumin Dithiothreitol	0.2 μM (0.2-10 μM) 20 nM (0.02-1 μM) 20 μg/mL (20-500 μg/mL) 20 nM (0.02-1 μM)

4.4 Conclusion

Table 2 & 3 summarize the studies mentioned in section 4.2 & 4.3. Based on this literature research, an optical approach is chosen for the design of the microfluidic device, namely absorbance measurements. Studies utilizing electrochemical approaches show low LoD's, however all studies still have uncertainties. They have not been tested in plasma/serum, on albumin or show interference of plasma components. DTNB is widely used for the detection of free thiols in plasma and is proven to be a reliable method. It is currently used at the UMCG. The major concern is to achieve sufficient sensitivity and a low enough LoD, as miniaturization of absorbance measurements leads to a decrease in sensitivity. If this problem arises, the use of nanoparticles or fluorescent probes can be explored to increase the sensitivity of the method.

5 Scope of Thesis

To achieve POCT, a device should be designed which is sample-in-answer out. The detection method of the microfluidic device will be based on the protocol as currently used in the UMCG, utilizing DTNB for the detection of free thiols. Therefore, the following steps should be incorporated into the microfluidic device:

1. Separation of whole finger-prick blood to plasma.
2. Dilution of plasma with 0.1 M Tris buffer, pH 8.2 (1:4 ratio).
3. Mixing of diluted plasma with 1.9 mM DTNB (4.5:1 ratio).
4. Filling of a reservoir with sufficient path length to enable absorbance measurements.

Figure 2 schematically shows the steps to be incorporated into the device. This thesis focuses on the last two steps of the protocol; the mixing of diluted plasma with DTNB and subsequent absorbance measurements. First, the thiol detection method using DTNB is miniaturized to sample volumes suitable for microfluidic devices. Based on these volumes, a microfluidic device will be designed with detection reservoirs, enabling on-chip absorbance measurements. At last, mixing of the diluted plasma with DTNB will be incorporated into the microfluidic device. Therefore, the final inlet sample will be diluted plasma.

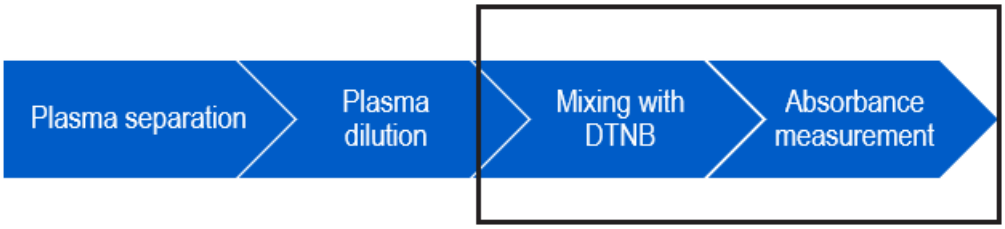

Figure 2: Steps to be incorporated into the microfluidic device.

6 Theory

6.1 Absorbance

Absorbance is a measurement of the quantity of light that is absorbed by a sample. Absorbance does not have a true unit, however it is often reported in 'Absorbance Units' (AU). [44] The absorption of light in a solution is dependent on the concentration (c) of the dissolved molecule, the specific molar extinction coefficient (ϵ) at a defined wavelength and the path length (l). This relation is given by the Lambert-Beer's law [45]:

$$A = log_{10}(\frac{I_0)}{I)} = \epsilon lc \tag{1}$$

A spectrometer measures the intensity of light that passes through a sample (I) and compares it to the intensity of the incident light (I_0). The ratio I/I_0 is called the transmittance, frequently expressed as a percentage. The more compound present in the sample, the lower the transmittance and the higher the measured absorbance. Light that is not detected at the detector, can be scattered or absorbed. The scattered part is determined by measuring blanks/background samples. These values are subtracted from the sample, before determining the concentration.

Absorbance measurements are most frequently performed using cuvettes with a fixed length (1 cm). However, when absorbance measurements are performed in a microplate, the path length differs per used volume, as depicted in figure 3. Additionally, different solutions can have different meniscus shapes and therefore different path lengths while being of the same volume.

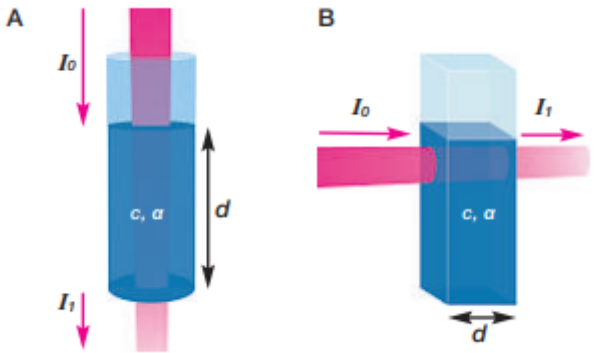

Figure 3: A) Absorbance measured in a microplate well B) compared to a fixed path length in a cuvette. Reprinted from [46]

With known extinction coefficient and path length, the concentration of a sample can be calculated using the measured absorbance via c = A /(ϵ * l). [47] The molar extinction coefficient represents the capacity of a substance to absorb light of a specific wavelength. It is therefore a substance- and wavelength dependent value. Studies have shown that the molar extinction coefficient of TNB is 14,150 M^{-1} cm^{-1} at 412 nm. This coefficient is not affected by changes in pH between 7.8-8.6. [48] The Lambert-Beer law can only be used for the determination of the concentration when; 1) the compound to detect absorbs light at a specific wavelength, 2) the path length is known, 3) the molar extinction coefficient is known and 4) the absorbance of buffer reagents do not overlap with absorbance wavelength of the compound.

Particles or other compounds present in the sample that interact with light will affect the measured absorbance value and therefore disturb the measurement. In addition, particles suspended in solution will move around and even more increase the variability of the measurements. Therefore it is important to remove particles from measured solutions, this can be achieved by e.g. centrifuging. In the same way, air bubbles will increase the measured absorbance values, and are therefore unwanted. [49]

6.1.1 Calibration curve

Concentration of samples can also be determined using a calibration curve, a curve which shows the change in the output of an analytical instrument towards different concentrations of the compound. Known concentrations are plotted against their corresponding absorbance values. Linear regression gives an equation in the shape of y = ax + b, in which a is the slope, x is the measured concentration value, b is the intercept and y is the measured absorbance. Therefore, the concentration of the sample can be calculated with [50]:

$$c = \frac{y - b}{a} \tag{2}$$

6.1.2 DTNB

As mentioned in the literature study, DTNB is often used for the detection of free thiol levels. DTNB has an oxidizing disulfide bond that is reduced in the presence of free thiols, releasing one molecule of 5-thio-2-nitrobenzoic acid (TNB^-), as depicted in figure 4. TNB^- ionizes to the TNB^{-2} dianion in water at neutral and alkaline pH. TNB^{-2} is a yellow coloured product with a maximal absorption at 412 nm. The reaction is stoichiometric; the presence of one mole of thiol will lead to the release of one mole of TNB. DTNB is suitable for free thiol detection, as it reacts specifically with sulfhydryl compounds, has a high molar extinction coefficient, is water-soluble and has a short-reaction time. Therefore the free thiol concentration in a sample can be determined by measuring the absorption at 412 nm before and after addition of DTNB. [51]

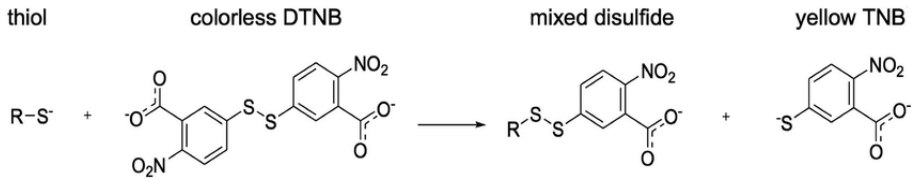

Figure 4: Reaction of DTNB with a free thiol. Reprinted from [52]

6.2 Capillary-driven microfluidics

To design a POC device, no external pumping equipment should be required for the operation of the device. The device should be portable and easy to use. Capillary-driven microfluidics are devices which work on the principle of capillary action without requiring any external mechanisms, making it very interesting for POC devices. Capillary pressure can act as both an opposing and driving force, enabling fluid manipulation inside the device when playing with the dimensions and wettability of the channels. [53]

6.2.1 Capillary Pressure

Capillary pressure (P_c) is based on the surface tension of a liquid and the wettability and geometry of the channel. The capillary pressure arises at the liquid-air interface in a microchannel as a result of surface tension of the liquid and the contact angles between the liquid and the channel walls. The Young-Laplace equation [54] gives the relation between the contact angle, microchannel dimensions and capillary pressure and can be expressed for a rectangular microchannel as follows:

$$P_c = -\gamma[\frac{cos(\theta, t) + cos(\theta, b)}{h} + \frac{cos(\theta, l) + cos(\theta, r)}{w}] \tag{3}$$

Where P_c is the capillary pressure, γ is the surface tension of the liquid, h is the channel height, w is the channel width and θ_t, θ_b, θ_l, θ_r are the contact angles of the liquid with respectively the top, bottom, left and right channel walls (see Fig. 5). The Young-Laplace equation shows that as the microchannel dimensions decrease, the capillary pressure increases. Therefore, when altering the dimensions of a microfluidic channel, you can adjust the capillary pressure and subsequently the flow within the device. Very high capillary pressures can be obtained in channels of small dimensions, increasing the pull on the liquid. In microchannels with low height-to-width ratios, the flow is driven primarily based on the interaction of the liquid with the top and bottom microchannel walls. [54]

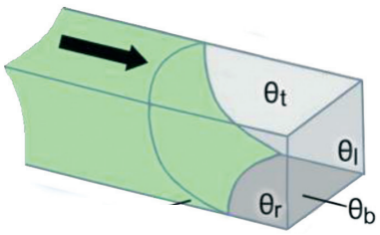

Figure 5: Liquid filling of microchannel. Reprinted from [54]

6.2.2 Contact angle

A surface is wettable when the contact angle of liquid on that surface is lower than 90 degrees. These materials are described as hydrophilic; they have affinity for water and are easily wetted. Hydrophobic materials have no affinity for water and are not easily wetted, therefore having contact angles with aqueous fluids larger than 90 degrees. [55] When a microchannel is fabricated of wettable surfaces, a concave liquid-air interface is generated and a negative capillary pressure is present that will suck the liquid into the channel. Contact angles lower than 60 degrees are preferred to ensure sufficient filling of the channels. When contact angles approach 90 degrees, a single imperfection in the microchannel can alter the contact angle and disrupt the flow. Therefore, contact angles lower than 60 degrees are preferred to ensure sufficient filling of the channels. [54]

PDMS is often used for the fabrication of microfluidic devices due to its optical properties, easy fabrication and tunable surface properties. [56] However, PDMS is naturally hydrophobic and therefore not suitable for capillary-driven microfluidic devices. Therefore, plasma treatment is used to produce usable hydrophilic PDMS substrates with a contact angle below 60 degrees. [57]

6.3 Trigger Valves

Trigger valves are structures that enable flow stoppage and subsequent liquid release, using only capillary pressure. Due to a sudden change in the liquid front meniscus, the capillary pressure will decrease and possibly (temporarily) stop the fluid flow. No external equipment is required for this valve, it is solely based on a change in capillary pressure. This makes this type of valve attractive for POC applications. [58] For microfluidic applications, it is important that there is accurate control of liquid flow, ensuring that multiple reagents reach the reaction or mixing structure simultaneously. Trigger valves ensure that fluids will only enter the detection chamber/mixing component, when both fluids are present in the device. This prevents inaccurate mixing or different ratios of mixing per device. These trigger valves also prevent bubbles from being created. [55]

This change in capillary pressure can be achieved by either altering the channel dimensions or wettability. Changes in wettability, and thus contact angle, can be achieved by hydrophilic and hydrophobic patterning. This approach is less attractive due to the addition of an extra step to the fabrication process of microfluidic devices. The second approach, altering the channel dimensions, often relies on a sudden expansion of the microchannel. This changes the radius of the meniscus curvature, decreasing the magnitude of the capillary pressure. This approach is easier in fabrication, as no special surface treatment is necessary. [55] When altering the dimensions of the channel, consequently the capillary pressure is altered, as the capillary pressure is scaled proportional to the inverse of the smallest dimension. The sudden increase in cross section will make it energetically unfavorable for the liquid to flow into the wide channel. Therefore, by drastically increasing the dimensions, a pressure barrier can be created which stops the fluid. [54] The incorporation of trigger valves in POC devices enables a walk-away format; the user can pre-load samples and reagents and subsequently start the assay at a time of their choosing, without any pressure of strict time windows.

Chen et al. [59] gives the following formula for the 3D model of the pressure barrier dP created by a sudden expansion:

$$dP = \frac{2\gamma}{w}[(-\frac{w}{h})cos\theta_c + (\frac{cos\theta_c - \frac{\alpha_w sin\beta}{sin\alpha_w}}{-cos\beta + \frac{sin\beta}{sin\alpha_w}(\frac{\alpha_w}{sin\alpha_w} - cos\alpha_w)})] \tag{4}$$

Where w is the width of the channel, h is the height of the channel, θ_c is the contact angle of the fluid with the channel, α_w is the circular arcs angle in width directions and β is the angle of expansion. When β is equal to 90 degrees, $\alpha_w = \theta_c$.

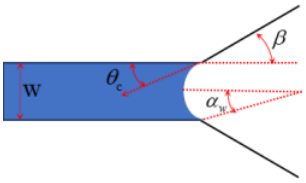

Figure 6: Sudden expansion of a microchannel, showing the angle of expansion (β), the contact angle (θ_c), the circular arc angle in the width direction (α_w) and the width of the channel (w). Reprinted from [55]

6.3.1 Two-level trigger valves

The first trigger valves (one-level trigger valves) designed were based on the junction of two microchannels (fig 7A); fluids are stopped at the junction until all microchannels are filled. However, these structures were not reliable, prone to spontaneous leaking and required very high aspect ratios (h/w = 12.5) and small dimensions.

To increase the reliability of the valves, two-level trigger valves were developed (fig 7B). [54] A narrow channel intersects a deeper channel, expanding both in vertical and horizontal direction. This is in contrast with the one-level trigger valves, which only expand horizontally (in width). The fluid in the narrow channel can be triggered by flowing a liquid through the deep channel, enabling mixing. [58] Two-level trigger valves can be designed with larger dimensions when compared to one-level trigger valves, reducing fabrication constraints. [54] Multiple studies utilize a hydrophobic PDMS cover to increase the efficiency of the trigger valve, as it prevents creeping of the liquid along the top. [58]

Olanrewaju et al. [60] studied the fabrication of trigger valves using 3D printing and PDMS replication, as most of the two-level trigger valves studied are fabricated in the clean room with small dimensions. They were able to fabricate trigger valves with dimensions up to 80 times larger than cleanroom fabricated ones. They studied different geometries of trigger valves and concluded that a height difference of minimally 300 μm is needed to ensure a 100% success rate of the valve. They observed that channels with low (<1) or high (>5) height-to-width ratios resulted in leaking of the valve. They tested up to a height of 1 mm for the narrow channel. They use a hydrophobic PDMS cover to prevent creeping of the fluid along the top surface.

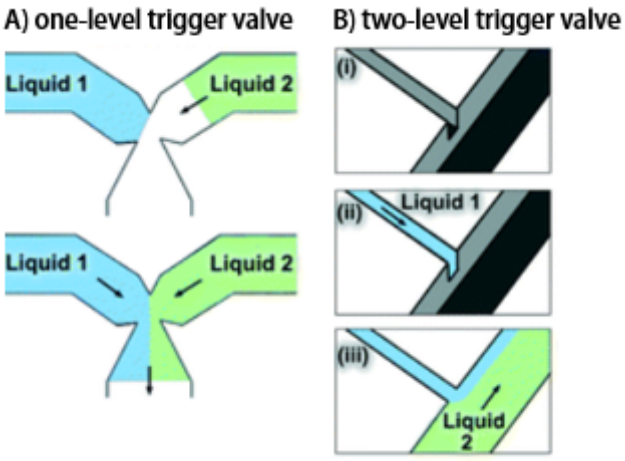

Figure 7: A) one-level trigger valve B) two-level trigger valve. Adjusted from [55]

6.4 Microfluidic Mixing

For many microfluidic applications in diagnostics, mixing is an important step. It is of importance that when measuring free thiols with DTNB, the diluted plasma and DTNB sufficiently mix. However, mixing is a challenge in microfluidics due to the small dimensions and therefore laminar flow.

6.4.1 Reynolds number

The Reynolds number (Re) predicts the flow patterns of fluids, as it is the ratio of inertial forces to viscous forces. Low Re represent laminar dominated flows, high Re represent flows that tend to be turbulent. The Reynolds number for flow in a channel can be calculated with the following formula:

$$Re = \frac{\rho v L}{\mu} \tag{5}$$

Where ρ is the density of the fluid, v is the flow velocity, L is the characteristic length and μ is the dynamic viscosity of the fluid. [61] The characteristic length is defined as A/P_w where A is the cross-sectional area of the channel and P_w the wetted perimeter at the cross section. [62]

When a channel has small dimensions, as is the case in microfluidics, Re will be low and therefore the flow is dominated by laminar flow. Thus, mixing occurs primarily due to diffusion, which is a slow process. This explains why mixing is a challenge in microfluidics, as mixing occurs over short distances. [63]

6.4.2 Microfluidic Micromixers

A great number of studies have been performed studying approaches to enhance the mixing efficiency in microfluidics. Microfluidic mixing approaches can be divided into two major categories; active and passive mixing.

Active mixing requires an external energy source to accelerate the diffusion process e.g. pressure gradients, electrical voltages or integrated mechanical mixing elements. They frequently require an external power source/equipment and tend to be harder to fabricate. This makes them less attractive for POC applications compared to passive micromixers. [64]

Passive micromixers require no external energy source and are therefore suitable for POC applications, they mostly rely on increasing the contact area and contact time between fluids. [63] Passive mixing is obtained through alterations in the structure, surface properties or configuration of microchannels. The mixing structure is incorporated into the device during fabrication and does not require any action from the user, making them less expensive and more convenient than active micromixers. There are multiple approaches possible to achieve passive mixing. [65]

6.4.3 Passive micromixers

The most basic micromixers are T- and Y-shaped channels, which bring together two different fluids in a larger channel. Mixing solely depends on diffusion in these configurations, therefore mixing is slow and requires a long mixing path. This traditional design can be improved by splitting and combining the streams at multiple points, increasing the contact area between the two fluids. [65] Another approach is the use of serpentine or twisted channels. This approach is suitable for fluid streams at moderate Re, but inefficient at low Re (1-40). [66] These geometries generate cross-sectional flows and induce chaotic advection, due to twisting of the interface between the two fluids [67]. Chaotic advection can also be achieved using patterned grooves or ridges, which induce rotational flows. Staggered herringbone mixers are used frequently, they consist of a repeated pattern of grooves on the bottom of the microchannel. These grooves are composed of two rectangles with different lengths; the short one spans one-third of the channel and the longer one two-third of the channel. The angle between the two intersecting grooves is set at 90 degrees in most designs. One mixing unit consists of two sets of herringbone grooves, the two sets are mirrored across the centerline of the channel, to increase the chaotic advection. [61] The number of grooves per half unit varies between 4 and 6. [68] Various other approaches are possible, such as the incorporation of embedded barriers, slanted wells or adjustments in surface chemistry such as hydrophobic patterning. However, these approaches make the fabrication process more complex, increasing the costs of the device. [63]

7 Materials & Methods

7.1 Off-chip method validation

7.1.1 Standard Protocol DTNB

The exact protocol as used at the UMCG for free thiol detection can be found in appendix B. Plasma samples were diluted 1:4 with 0.1 M Tris buffer (pH 8.2) (Merck KGaA, Darmstadt, Germany). 90 μL of diluted plasma samples were pipetted into a 96 wells plate (Greiner) in triplo. After measuring background absorption at 412 nm with a reference measurement at 630 nm, 20 μL 1.9 mm DTNB (SigmaAlderich Chemie GmbH, Steinheim, Germany) in 0.1 M phosphate buffer (pH 7) was added to the samples. Absorbance was measured again after incubation time of 20 minutes in the dark at room temperature using a plate reader (SpectraMax ID3). Concentrations were determined by parallel measurement of a L-Cystein (SigmaAlderich Chemie GmbH, Steinheim, Germany) calibration curve (15.625 to 1000 μM final concentrations) in a 0.1 M Tris, 10 mM EDTA solution (pH 8.2) (Serva, Heidelberg, Germany). Absorbance values were corrected by subtracting the reference measurements at 630 nm from the 412 nm measurements, after which the background measurements were subtracted from the DTNB measurements.

7.1.2 Sample miniaturization

To be able to perform the detection of free thiols on a microfluidic device, a lower sample volume is required than the 90 μL 1:4 diluted plasma used in the standard protocol.

First, experiments were performed on PBS spiked with L-Cystein. 1 mM L-Cystein in PBS was serially diluted to obtain final concentrations (15.625-1000 μM). 4 μL, 6 μL and 10 μL sample were 1:4 diluted in 0.1 M Tris buffer (pH 8.2) to obtain respectively volumes of 16 μL, 24 μL and 40 μL. These volumes were added in triplo for each concentration and volume in a 384 wells plate (Nunc). The same protocol as described in section 7.1.1 was followed for the determination of free thiol levels, DTNB volumes were adjusted to maintain similar ratios. The exact protocol can be found in appendix C.

After successful finalization of this experiment, experiments were performed on small volumes of plasma. Plasma samples with known thiol levels were provided by the UMCG. Plasma samples were stored at -80 degrees before use, maintaining the thiol levels. Again samples of 4 μL, 6 μL and 10 μL were used after 1:4 dilution in 0.1 M Tris buffer (pH 8.2). The volume with the smallest variation and compatible LoD and Limit of Quantification (LoQ) was used for a larger scale experiment; 8 x 384 wells plates were filled with 6 diluted plasma samples, again following the protocol as outlined in appendix C.

7.1.3 Colorimetric Detection

A L-Cystein standard curve (15.625-1000 μM), a 1:4 diluted L-Cystein standard curve (15.625-1000 μM) and two 6 μL 1:4 diluted plasma samples in 0.1 M Tris buffer (pH 8.2) were pipetted in triplo into a 384 wells plate, all with a total volume of 24 μL per well. Free thiol levels for all samples were determined using the protocol as outlined in appendix C. Images of the wells were taken before and after the addition of DTNB using the EVOS microscope (EVOS m5000, Invitrogen, Thermo Fisher Scientific, Massachusetts, USA) (amplification 4x). ImageJ was utilized to calculate the mean intensity of each well. The mean intensity was plotted against the free thiol levels of the samples.

7.2 On-chip absorbance measurements

After the method was validated off-chip, a microfluidic device was designed to perform on-chip absorbance measurements. The design of this first microfluidic device was focused on solely facilitating the absorbance measurements. Sample preparation steps such as mixing of the plasma with DTNB, plasma dilution and plasma separation were all performed off-chip.

7.2.1 Determination of path length

The Lambert-Beer Law states that the path length is an important factor when measuring absorbance. When performing absorbance measurements in well plates, the path length differs greatly per used volume. Therefore, it is important to know the path length of the sample volume used in previous experiments, as this path length should be utilized for the design of the microfluidic device. Path length can be calculated using a mathematical approach (calculating the height of the sample from the known dimensions of the well and the volume) or with the water peak correction method. The latter method is chosen, as this method corrects for pipetting errors and the shape of the fluid menisci. In addition, no assumptions of the well geometry are made.

Water is transparent from 200 to 900 nm, however in the near infrared (NIR) a distinctive absorption peak is visible near 977 nm. When measuring the absorption of water ($A_{reference}$) for a path length of 1 cm at 977 nm, the path length can be determined from the measured absorbance of a water sample (A_{sample}) with unknown path length. Due to the absorption of water being temperature dependent, sample measurements may be subject to error if there are fluctuations in the temperature. To avoid this error, a reference measurement was conducted at 900 nm and deducted from the absorption at 977 nm. The following equation was used to calculate the path length (d_{sample}) of the aqueous sample [46]:

$$d_{sample} = \frac{(A_{977} - A_{900})_{sample}}{(A_{977} - A_{900})_{reference}} * 1cm \tag{6}$$

29.34 μL of 0.1 M Tris buffer (pH 8.2) was pipetted into the wells in triplo, after which the absorbance was measured at 900 nm and 977 nm using the plate reader.

7.2.2 Design Chip Holder

A chip holder was designed using SolidWorks (Fig 8), to be able to perform on-chip absorbance measurements using the plate reader. The chip holder was designed to resemble the dimensions of a Nunc 384 wells plate. A cut-out is fabricated in the holder, to ensure that the reservoirs of the microfluidic device are located at the precise location where normally measurements on wells are performed. The cut-out is designed to fit a microscopic glass slide (25 mm x 75 mm), with a marge of 2 mm on all sides. An edge of 4 mm is present on all sides for the chip to rest on. The depth of a Nunc 384 well plate is 11.7 mm, therefore the chip holder is designed to hold the chip at a depth of 12.7 mm, compensating for the 1 mm height of the microfluidic glass slide. Detailed drawings of the chip holder design can be found in appendix D.

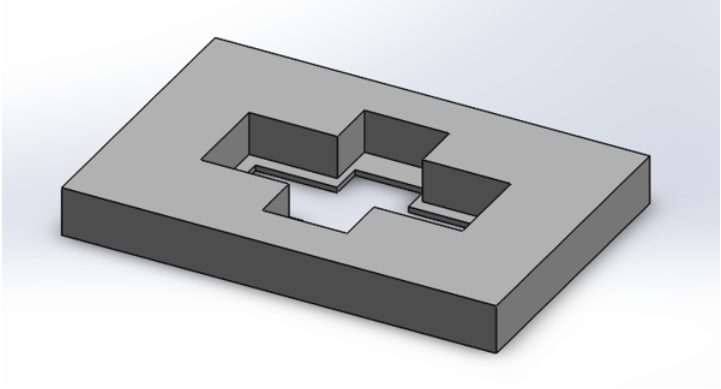

Figure 8: 3D View of chip holder design in SolidWorks.

7.2.3 Design Master Mould

A positive mould was designed in SolidWorks for the fabrication of PDMS microfluidic devices. The PDMS device fabricated with this mould contains 7 reservoirs which serve as detection chambers for the absorbance measurements. The reservoirs have a height of 3.06 mm, corresponding to the calculated path length. Appendix E shows the initial design of the master mould, this design was adjusted to obtain the design presented here. The initial design did not contain an outlet, resulting in problems with complete filling of the reservoirs and creation of air bubbles in the reservoirs. Air bubbles greatly affect the absorbance measurements, as they reflect light. Furthermore, the rectangular reservoirs were transformed to cylindrical reservoirs, eliminating the sharp edges which could also play a role in air bubble formation. Figure 9 shows the final design of the master mould. Reservoirs 1, 2, 3 and 4 have a height of 3.06 mm, as calculated with water peak correction. To study if absorbance measurements using a lower path length are feasible, reservoirs 5, 6 and 7 with a height of 2 mm were added to the mould. To study the effect of channel height on air bubble formation, various channel heights were incorporated in the mould. The channels of reservoir 1 and 2 have a height of 3.06 mm, matching the height of the reservoirs. The channels of reservoir 3 and 4 have a height of 2 mm. Channels of reservoir 5 and 6 have a height of 2 mm, matching the height of the reservoirs. The channels of reservoir 7 have a height of 700 μm. All channels have a width of 1 mm. The in- and outlet have a diameter of 0.75 mm, allowing entrance of a micro pipette tip.

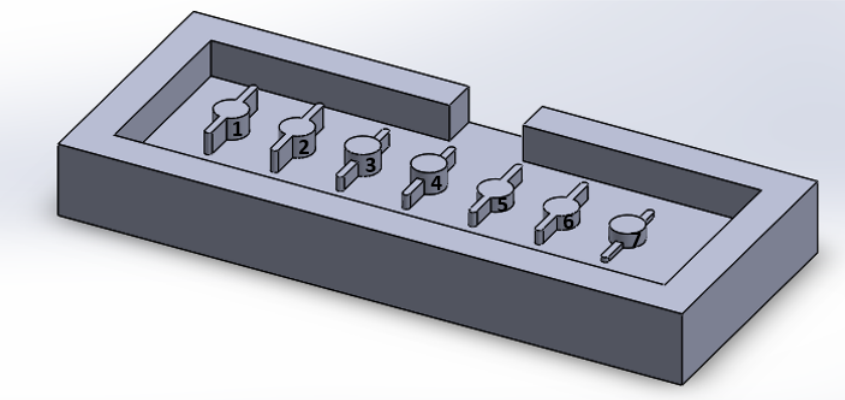

Figure 9: 3D View of master mould design in SolidWorks.

7.2.4 Fabrication

Master Mould

The commercially available software SolidWorks was used to design a master mould. This design was then fabricated by micromilling. The SolidWorks file was loaded in the milling machine, after which the program controlled the mill. A polymethylmethacrylate (PMMA) substrate was placed in the milling machine, from which the mill removed material based on the loaded file to create the master mould. After milling, the mould was cleaned using isopropyl alcohol (IPA) and rinsed with distilled water.

PDMS Devices

PDMS prepolymer and curing agents were mixed in a 10:1 ratio and degassed by placing the uncured polymer solution in the desiccator for 30 minutes. The mixture was poured in the master mould, after which the mixture was degassed again for 30 minutes. The mixture was then cured for a minimum of 2 hours at 60 degrees. The PDMS replicas were peeled off the mould, inlets and outlets were punched with a 0.75 mm punch. The PDMS replica and a microscopic glass slide were rendered hydrophilic in the plasma oven (CUTE, Femto Science, Besançon, France), after which they were bonded. Bonding was completed after 20 minutes in 60 degrees.

7.2.5 Testing PDMS devices

To validate that the plate reader performed measurements at the right locations, the inlets of a PDMS device were filled with 500 μM L-Cystein in 0.1 M Tris buffer (pH 8.2), mixed with 1.9 mM DTNB. Calibration curves were measured in duplo for both the 2 mm and 3 mm reservoir, using an L-Cystein standard solution (15.625 to 1000 μM final concentrations) in 0.1 M Tris buffer (pH 8.2), mixed with 1.9 mM DTNB in a 4.5:1 ratio. Results were compared with parallel measurements in a 384 wells plate.

Plasma samples were centrifuged (10 min, 10 rcf), the supernatant was 1:4 diluted with 0.1 M Tris buffer (pH 8.2). The sample was split into two separate eppendorfs, to one eppendorf 1.9 mM DTNB was added in a 4.5:1 ratio (diluted plasma:DTNB). The other eppendorf served for background measurements. Both samples were pipetted into the inlets connected to reservoirs, each PDMS device containing both background and DTNB measurements for both 2 mm and 3 mm path length. Measurements were performed by placing the PDMS device in the chip holder in the plate reader. The same plasma samples were simultaneously measured in a 384 wells plate. Figure 10 shows the workflow schematically.

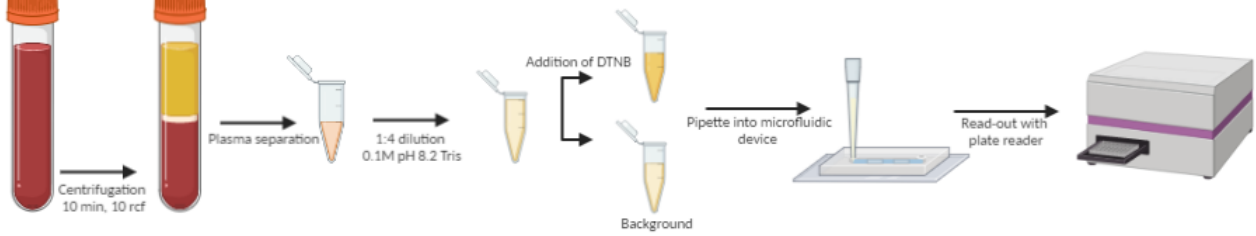

Figure 10: Workflow on-chip plasma measurements. Created with biorender.com

7.3 Validation

Results from both off-chip and on-chip measurements were analysed using Excel. To determine the precision, both repeatability and reproducibility were expressed as intra-coefficient of variation (CV) and inter-CV. The CV was calculated by dividing the standard deviation (SD) by the mean, multiplied by 100. The intra-assay CV, variation within 1 plate, was calculated per triplo and an average intra-CV per plate was calculated. Intra-CV's below 10% are acceptable. The inter-CV, the plate-to-plate variation, was calculated using the SD of plate means and the mean of plate means. Inter-CV's below 15% are generally acceptable. [69]

From the calibration curves, the LoD and the Limit of Quantification LoQ were calculated. The LoD is defined as the lowest concentration of an analyte in a sample that can be consistently detected with a stated probability of 95%. The LoD was calculated with the following formula [70]:

$$LoD = 3.3 * \frac{\sigma}{a} \tag{7}$$

Where σ is the SD of the intercept and a the slope of the calibration curve. The LoQ is defined as the lowest concentration of an analyte that is possible to be determined with an acceptable precision and accuracy; the signal is statistically different from the background. The LoQ was calculated with the following formula [70]:

$$LoQ = 10 * \frac{\sigma}{a} \tag{8}$$

The slope is calculated over the interval of 0-250 μM, the standard error (SE) of the intercept is calculated over the interval of 0-500 μM. The SD of the intercept is calculated from the SE of the intercept with the following equation: SD of intercept = SE of intercept * $\sqrt{N}$, where N is the number of tests. [71]

7.4 Trigger Valves

7.4.1 Design Trigger Valves

Equation 4, from Chen et al. [59] was utilized to calculate the pressure barrier that is created at the intersection of the narrow and the deep channel. An expansion angle β of 90 degrees is utilized, therefore it can be stated that $\alpha_w = \theta$. For this calculation, a surface tension of 72 mN/m is assumed; the surface tension of water at 25 degrees. A contact angle of 31 degrees is assumed between the liquid and the plasma treated PDMS. [60] When a width of 300 μm is chosen for the narrow channel, a height of 1250 μm, 900 μm, 700 μm and 500 μm lead respectively to a pressure barrier of 50 Pa, 70 Pa, 90 Pa and 126 Pa. However, this equation solely takes the horizontal (width) expansion into account. In our design, an additional vertical (height) expansion will be present. Therefore, these calculated pressure barriers are the minimal values, in our design they will increase due to the two-level expansion.

To study the influence of the vertical expansion of the channel, four different trigger valve structures were fabricated in one master mould (Fig. 11). Four different heights (h) of the narrow channel were chosen; 1250 μm, 900 μm, 700 μm and 500 μm, corresponding to a difference in height (Δh) of respectively 750 μm, 1100 μm, 1300 μm and 1500 μm. w_1 (300 μm) and w_2 (1000 μm) are constant for all 4 trigger valves. The height of the deep channel, with which the narrow channel intersects, is set to 2 mm. Detailed drawings of this master mould can be found in appendix F.

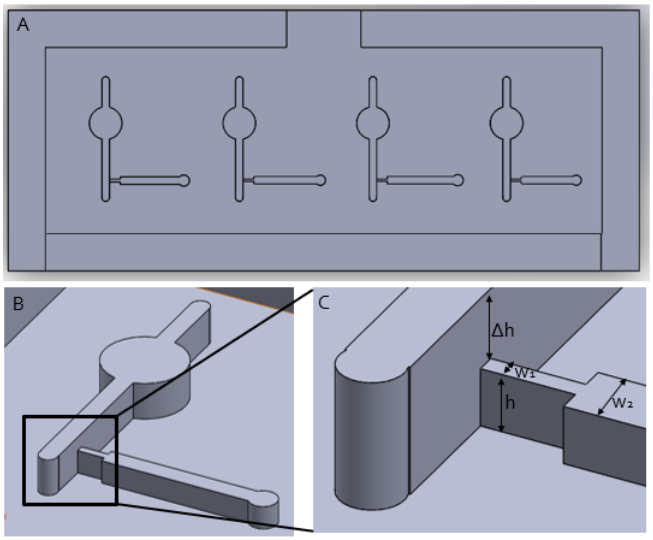

Figure 11: A) SolidWorks design of master mould B) focused on one trigger valve structure of mould C) Zoom-in showing height (h), height difference (Δh) ,widths of the narrow channel, small part (w_1) and wider part (w_2).

7.4.2 Fabrication Trigger Valves

Master Mould
A PMMA master mould was fabricated as described in section 7.2.4.

PDMS Devices
Fabrication of PDMS devices occurred as described in section 7.2.4. In addition to PDMS devices sealed with a hydrophilic glass cover, PDMS layers were sealed with a hydrophobic PDMS cover. This hydrophobic cover was created by coating a microscopic glass slide with PDMS and curing it at 60 degrees for 45 minutes, after which the sticky PDMS layer was placed on the PDMS layer containing the structures. Bonding was completed after 1.5 hour curing in 60 degrees. All in- and outlets were punched using a 3 mm punch instead of 0.75 mm. Filter paper was added to the outlet.

7.4.3 Testing of Trigger Valves

Images of the intersection of the narrow and deep channel were taken with the microscope (Leica DM 6000M), to inspect if micro milling and PDMS replication is suitable for the development of

these fine structures. The microscope was used to measure the difference in height between the narrow and deep channel for all 4 designs.

Experiments were performed on the 4 different designs to determine which height differences provide high success rates, for both the devices sealed with a hydrophobic and a hydrophilic cover. Trigger valve success is defined as when a valve holds the liquid for at least 10 minutes without leakage. The trigger valves were tested using aqueous food dye solutions. First, the narrow channel was filled with a blue food dye. After 10 minutes, the deep channel was filled with a yellow food dye, to observe if the blue liquid is triggered by the filling of the deep channel, allowing mixing.

7.5 On-chip mixing

7.5.1 Design Microfluidic Mixer

During the testing of the trigger valves, it was observed that microchannels were immediately filled after pipetting the liquid into the inlet, indicating high fluid velocities. Furthermore, the liquid in the channels and reservoirs turned green, indicating that mixing already took place over short distances without incorporation of a mixer structure. Therefore it is assumed that the flow in the microchannels has a moderate Reynolds number (> 40) and a serpentine mixer can be used. However, it should be noted that this is an assumption and experiments should be performed to assess the efficiency of the serpentine mixers.

A positive mould was designed using SolidWorks. The mould consists of 4 structures. All structures contain a trigger valve with a narrow channel height of 500 μm, corresponding to a height difference of 1500 μm. All deep channels have a width of 700 μm and a height of 2000 μm. On the left, two identical serpentine mixer structures are present (Fig. 12B), they contain 3 rectangular mixing elements that are located after the trigger valve. On the right part of the mould, two straight channels with a total length of 16 mm are present. The bottom straight channel has a staggered herringbone structure incorporated onto the deep channel (Fig. 12C). The grooves are 100 μm wide and 300 μm high. The longer leg of the groove spans two-third of the channel, the shorter leg one-third. The angle between the short and long leg is 90 degrees. The mixer consists of 4 sets of herringbone grooves, each set is followed by a complementary set mirrored across the center line of the channel. 1 set consists of 6 herringbone grooves, with an inter-groove spacing of 160 μm. The distance between two sets is 600 μm. Drawings with dimensions of both structures can be found in appendix G

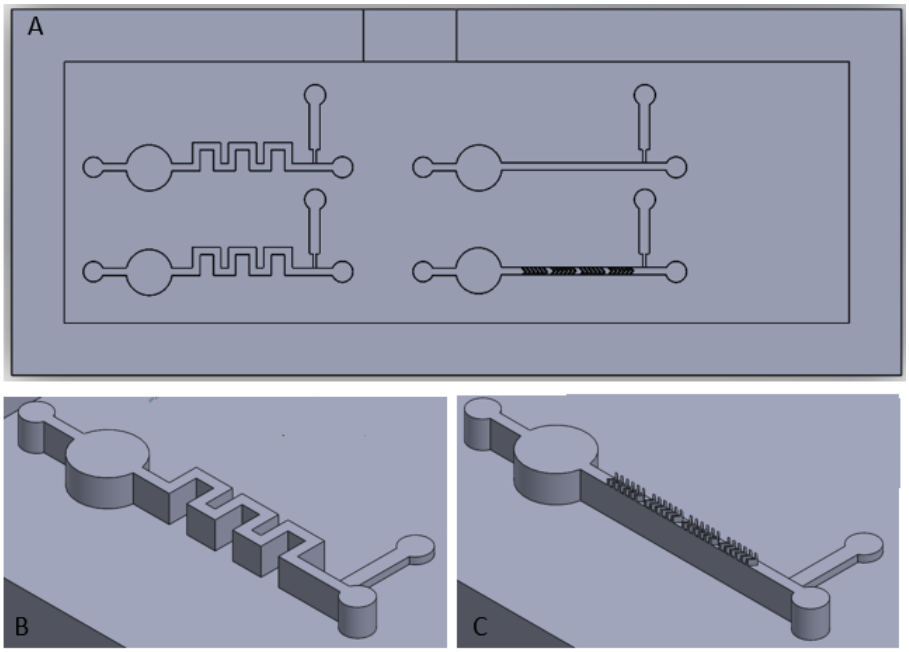

Figure 12: A) 3D view in SolidWorks of master mould B) Zoom in on serpentine mixer C) Zoom-in on staggered herringbone mixer.

7.5.2 Fabrication Mixer

Master Mould
A PMMA Master Mould was fabricated using micro milling as described in section 7.2.4.

PDMS Devices
Fabrication of PDMS devices occurred as described in section 7.2.4. Instead of a 0.75 mm punch, a 3 mm punch was used to punch the in- and outlets. Filter paper was added to the outlet of the device.

7.5.3 Testing of mixer

Images of the herringbone structures were taken using the microscope (Leica DM 6000M), to inspect if micro milling and PDMS replication are a suitable approach for the fabrication of herringbone grooves. A blue food dye was pipetted into the inlet of the narrow channel. After 10 minutes, a yellow food dye was slowly pipetted into the inlet of the deep channel until the filter paper in the outlet was reached. Pictures were taken of the PDMS device to assess the efficiency of mixing.

8 Results & Discussion

8.1 Off-chip Method Validation

8.1.1 Standard Protocol DTNB

At the UMCG, serum and plasma samples were measured in triplo in 96 well plates. These measurements gave an average intra-CV of 1.9%.

8.1.2 PBS Spiked with L-Cystein

The calculated free thiol levels of the serial diluted 1 mM L-Cystein in PBS for the volumes of 4 μL, 6 μL and 10 μL were compared to the expected concentrations. In the relevant range (125-1000 μM), the measured and expected concentrations were comparable; all differences were below 4% for 6 μL and 10 μL and all below 6% for 4 μL. When calculating the SD and intra-CV, samples with a concentration between 31.25 and 1000 μM were taken into account. Lower concentrations have relative high variation and seem to be subject to noise and were therefore discarded. All three volumes showed acceptable repeatability, as their intra-CV's are far below 10% (Table 4). Elaborate results can be found in appendix H.

Table 4: Standard Deviation (SD), Intra-Coefficient of Variation (Intra-CV), Limit of Detection (LoD) and Limit of Quantification (LoQ) calculated for 4 μL, 6 μL and 10 μL PBS L-Cystein spiked samples.

Sample Volume (1:4 diluted)	SD (μM)	Intra-CV (%)	LoD (μM)	LoQ (μM)
4 μL	8.87	2.74	19.4	58.8
6 μL	6.80	2.31	15	45.5
10 μL	6.88	2.75	10.9	33.2

Table 4 shows the LoD and LoQ that were calculated from the calibration curves measured per sample volume. For all three sample volumes, the LoD and LoQ are far below the relevant range of free thiol levels (200-800 μM). Therefore, all three volumes are used in the low plasma volume experiments.

8.1.3 Low Plasma Volume

Plasma samples with a volume of 4 μL, 6 μL and 10 μL were 1:4 diluted in 0.1 M Tris (pH 8.2) and measured in a 384 wells plate. The intra-CV's were calculated, giving respectively 18.5%, 5.4% and 13.9%. 6 μL is the only sample volume with an acceptable intra-CV (below 10%), therefore this sample volume was used for the experiment at larger scale. This increase in CV might be explained due to the more complex composition of plasma when compared to PBS, containing many other components which can absorb or scatter light. Elaborate results can be found in appendix I.

Table 5 shows the average concentration (μM), SD and intra-CV of the 8 plates used for the detection of free thiol levels in 6 μL plasma samples. Intra-CV's should be less than 10%, which is the case for 7 out of 8 plates. The high intra-CV of plate 3 (12.7%) could be caused by a pipetting error. At such low working volumes, pipetting errors or different shapes of fluid menisci can greatly affect the measured concentration. The inter-CV is 10.5% (n=8). An inter-CV below 15% is generally acceptable, therefore from these results it is concluded that a plasma volume of 6 μL can reliably be used for the detection of free thiols using DTNB. All measurements were performed on control plasma samples, provided by the UMCG. Samples were measured both at the UMCG with the standard protocol and at the UT with the adjusted protocol. The average concentration measured at UMCG was 329.9 μM, at the UT an average concentration of 354.7 μM was found.

Table 5: Concentration (uM), standard deviation (SD) and intra-coefficient of variation (Intra-CV) values of 8 well plates filled with 6 μL plasma, 1:4 diluted to 24 μL.

Plate	1	2	3	4	5	6	7	8
Concentration (μM)	309	331	347	374	337	356	382	432
SD (μM)	13.2	5.3	44.1	16.2	19.2	9.1	26	2
Intra-CV (%)	4.3	1.6	12.7	4.3	6.7	2.5	6.8	0.5

8.1.4 Colorimetric Detection

The mean intensities calculated using ImageJ of the images of the wells were compared to the free thiol levels calculated from the absorbance measurements. For the calibration curve, an increase of intensity could be seen as the concentration increased. However, the relation was not linear. The same applied for the 1:4 diluted calibration curve; the increase of intensity with relation to the concentration was not linear. Six 6 μL plasma samples were 1:4 diluted, the measured concentration was plotted against the intensity found with ImageJ. No relation was found between free thiol levels and intensity, showing that intensity measurements are not as accurate as the absorbance measurements. Elaborate results can be found in appendix J.

8.2 On-chip Absorbance Measurements

8.2.1 Determination of path length

From absorbance values obtained with the water absorption experiments, the path length of the sample could be calculated (for a sample of 6 μL):

$$d_{sample} = \frac{0,088833 - 0,036}{0,057474 - 0,229938} * 1cm = 3.06mm$$

This value of 3.06 mm can still differ from the true path length, as the meniscus of diluted plasma could differ from the meniscus of Tris buffer. Plasma path length cannot be determined with this approach, as plasma also absorbs light at these wavelengths. Therefore a path length of 3.06 mm was chosen for the design of the microfluidic device, as it is the best estimation.

8.2.2 Fabrication Devices

The master mould and chip holder were successfully fabricated using the micro mill. PDMS devices were successfully replicated from the master mould. Figure 13 shows a PDMS device filled with blue food dye. When the height did not match the height of the reservoirs, there was incomplete filling of the reservoirs and often air bubbles were visible in the reservoirs. This problem did not occur in the channels and reservoirs which height matched; complete filling of the reservoirs occurred without any air bubble formation. Air bubbles greatly affect the absorbance measurements, as they scatter light. Therefore, for all next measurements only reservoirs 1, 2, 5 and 6 were taken into account. Reservoirs 3, 4 and 7 were not used in all following measurements.

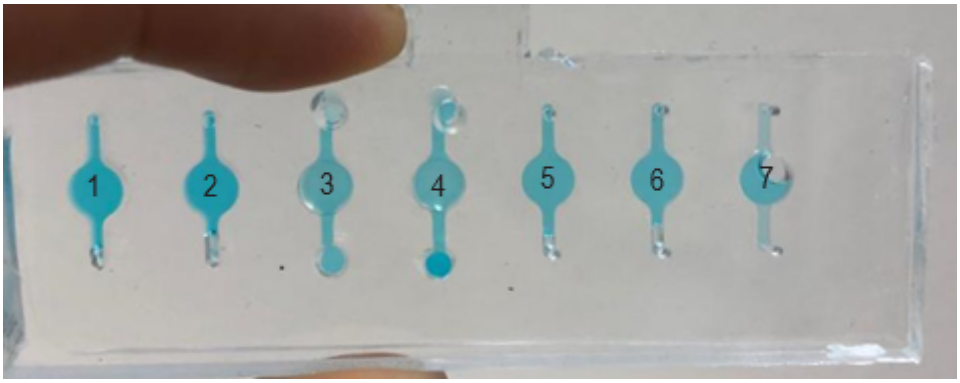

Figure 13: Image taken of the PDMS device containing 7 reservoirs for absorbance measurements, filled with blue food dye.

8.2.3 Testing PDMS devices

The measurement of the same sample (500 μM L-Cystein in Tris mixed with DTNB), divided over the reservoirs of the PDMS device, gave an intra-CV of 0.72%. This proves that the reservoirs are located at the correct positions in the plate-reader and the chip holder can be used for on-chip absorbance measurements.

Calibration Curve
Calibration curve measurements using the 2 and 3 mm reservoirs gave a linear relation between concentration and absorbance. For the 3 mm reservoir a LoD of 40.9 μM and a LoQ of 123.9 μM were calculated. For the 2 mm reservoir a LoD of 54.4 μM and a LoQ of 164.9 μM were calculated. For both path lengths the LoD and LoQ values are below the relevant range of free thiol levels (200-800 μM). Therefore, both 2 and 3 mm reservoirs were used for plasma sample measurements.

Plasma samples
6 PDMS devices were filled with the same 1:4 diluted 6 μL plasma sample. Each PDMS device contained a 2 mm and 3 mm reservoir filled with diluted plasma without DTNB (background) and with DTNB. Background measurements were subtracted from the DTNB absorbance measurements after which free thiol concentrations were calculated using the L-Cystein standard curve. Table 6 shows the concentration, SD and inter-CV obtained using the PDMS devices compared to the concentrations obtained using the 384 wells plate. Only of 4 PDMS devices the 2 mm reservoirs could be filled, due to fabrication errors (e.g. rupture of PDMS).

Results show that on-chip absorbance measurements result in a lower inter-CV (1.9% & 4.2%) compared to measurements performed in a 384 wells plate (6.24%). Elaborate results can be found in appendix K. This difference in CV can be explained by the fact that the on-chip absorbance is measured through a reservoir with constant path length. In the 384 wells plate, the shape of the meniscus and variations in fluid positioning in the well can increase the variability of the measurements. This variability is now eliminated due to a bordered detection reservoir with constant path length.

The concentrations determined using the 3 mm reservoir (406 μM) are on average 1.02 times higher than the concentrations determined using the 384 wells plate (396.6 μM), which is only a slight difference. However, the concentrations determined using the 2 mm reservoir (441.9 μM) are on average 1.11 times higher. This could be due to an error in the measurement of the standard curve in the 2 mm reservoirs. Both standard curves have only been measured once in the PDMS device, therefore an error in these experiments could have led to faulty concentration determinations. Further tests should be performed measuring multiple standard curves, to see if these values remain constant when measured on different days. Furthermore, the measurements in 2 mm reservoirs were only performed on 4 PDMS devices. Ideally, this experiment should be repeated using a higher number of PDMS devices. If a master mould is redesigned to contain only 2 mm reservoirs with 2 mm high channels, more samples can be tested within 1 PDMS device, fastening the process. With the current design, only 2 measurements per path length can be performed per PDMS device.

Table 6: Concentration (μM), Standard Deviation (SD) and Inter-Coefficient of Variability (Inter-CV) values of free thiol determination in a 2 and 3 mm reservoir and in a 384 wells plate.

	Concentration (μM)	SD (μM)	Inter-CV (%)
3 mm reservoir (n=6)	406	7.8	1.9
2 mm reservoir (n=4)	441.9	18.5	4.2
384 wells plate	396.6	24.8	6.24

8.3 On-chip sample preparation

8.3.1 Trigger Valves

Characterization

Figure 14 shows the image taken with a microscope of the intersection of the narrow and the deep channel, of the trigger valve with h = 1250 μm. Due to the use of the micro mill, the final structure differs from the original design, as the edges are more rounded instead of sharp. This results in a less sudden expansion, as the narrow channel already starts widening at the intersection.

The difference in height was determined for all 4 designs using the microscope. The height differences measured were 818 μm, 1.14 mm, 1.24 mm and 1.47 mm, corresponding to the designed height differences of 750 μm, 1.1 mm, 1.3 mm and 1.5 mm. Micro milling and PDMS replication of the designs results in slight modifications of the dimensions when compared to the initial design. However, all differences are below 100 μm. Slight differences were expected, as micro milling results in more rough and layered channel walls when compared to e.g. clean room fabrication.

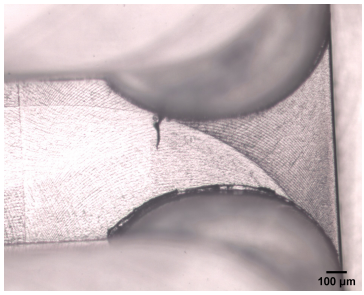

Figure 14: Optical microscope image of trigger valve intersection in PDMS device, at 2.5x magnification.

Testing of Trigger Valves

Inlets of the narrow channels were filled with an excess of blue food dye (Fig 15A). The trigger valves with a height difference of 1100 and 1500 μm had a success rate of 100% (n=8); none of the valves showed any leakage of the blue food dye after 10 minutes. The trigger valves with a height difference of 750 and 1100 μm showed a success rate of 87.5% (n=8). No differences were found between PDMS devices with a hydrophobic or hydrophilic cover. The lower success rate of the trigger valve with a height difference of 750 μm can be explained due to the fact that the lowest pressure barrier is present at this intersection. The lower success rate of the trigger valve with a height difference of 1100 μm is more difficult to understand, as you would expect that all trigger valves with a height difference above a certain value would give a similar success rate. It could be due to a fabrication error or if the liquid was inserted from a higher distance into the inlet, generating a higher pressure.

After 10 minutes, the yellow food dye was pipetted into the inlet of the deep channel, triggering the blue food dye in the narrow channel. Blue food dye entered the deep channel until the inlet reservoir of the narrow channel was emptied. Emptying of the reservoir only occurred when a filter paper was inserted into the outlet of the deep channel, therefore liquid actuation is needed to induce emptying of the narrow channel. As you can see in figure 15B, the narrow channel itself stays filled. Therefore, by filling the reservoir of the narrow channel with the amount of fluid you want to mix with the fluid in the deep channel, you have control over the mixing ratio.

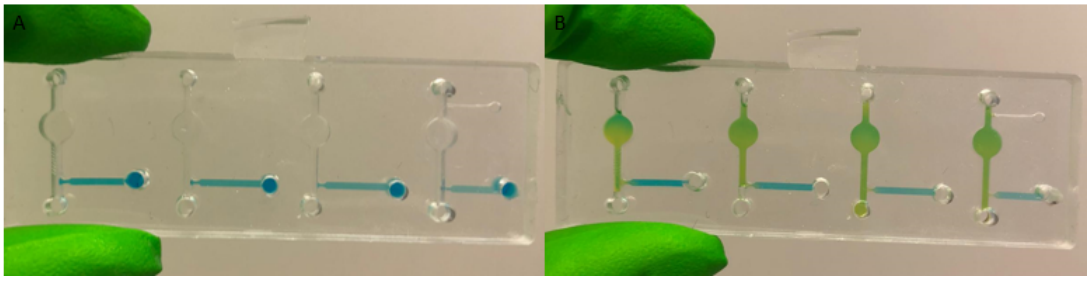

Figure 15: A) Narrow channel of two-level trigger valve is filled with blue food dye B) After 10 minutes, the deep channel is filled with yellow food dye, triggering the flow of the blue food dye.

8.3.2 Mixing

Characterization

As can be seen in figure 17A, the serpentine mixers (structures on the left) are not similar to the SolidWorks design. The use of a micro mill in combination with too small distances between the channels has probably led to fusion of the channels. The structures on the right, the straight channels, look as expected. Figure 16 shows the image taken with a microscope of the herringbone structure in PDMS, fabricated using the master mould (Fig. 12A). The structure shows no fabrication errors, leading to the conclusion that micro milling of a master mould in combination with PDMS replication can be used for the fabrication of herringbone structures at these dimensions.

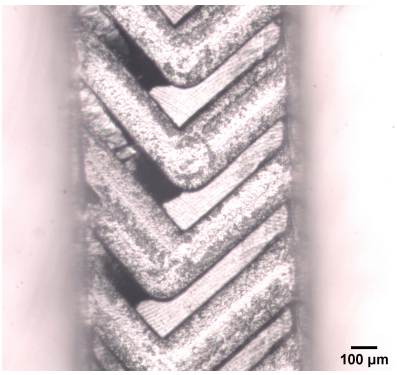

Figure 16: Optical microscope image of herringbone structure in PDMS device, at 2.5x magnification.

Testing of Mixing Structures

No leakage of the narrow channels was observed after filling with blue food dye (Fig 17A). After 10 minutes, yellow food dye was pipetted into the inlet of the deep channel. When yellow food dye was pipetted into the two serpentine mixers, yellow food dye partly went into the narrow channel containing the blue food dye. Only after reaching the filter paper in the outlet of the device, emptying of the inlet of the narrow channel occurred. Therefore, this design is discarded. To see if a serpentine mixer is suited for our device, a new master mould should be designed with larger distances between the channels to ensure correct fabrication.

The right structures both contain a long straight channel, the bottom structure has a herringbone pattern incorporated onto this straight channel. When the yellow food dye was pipetted into the inlet of the deep channel, the blue food dye entered the deep channel. However, as you can see in figure 17B, also some yellow fluid mixes with the blue liquid in the narrow channel. However, this is significantly less volume when compared with the serpentine mixers. There was clear mixing of the yellow and blue liquid, as the liquid in the deep channel turned green. When the filter paper was reached (Fig. 17C), the inlet of the narrow channel was fully emptied. No significant difference between the two channels regarding mixing efficiency was observed, therefore it is concluded that the current herringbone structure does not noticeably increase mixing efficiency. Mixing could be further enhanced by increasing the dimensions of the staggered herringbone structure, resulting in greater disruption of the laminar flow.

It was observed that mixing was most optimal when the yellow food dye was slowly pipetted into the inlet of the deep channel. This is not expected, as higher velocities result in more turbulent flow and increase mixing. However, a slow flow resulted in a more constant release of the blue food dye from the narrow channel. When very high velocities were reached, yellow food dye entered the narrow channel in some cases. Therefore, it could be beneficial if the diluted plasma enters the deep channel at a lower velocity. This is difficult to control when manually pipetting the liquid into the inlet. Furthermore, when manually pipetting the liquid into the inlet of the deep channel, there will be no consistent flow, as it is difficult to exactly repeat the manual pipetting action. A capillary pump can be designed to obtain a certain flow rate in the microchannels, as the flow rate of a liquid in a capillary system is partly determined by the total flow resistance and the capillary pressure in the capillary pump. [72] It could be interesting to look into the replacement of the filter paper with a capillary pump to obtain a slower and pre-set flow rate in the deep channel. Other studies [58] [73] designing microfluidic trigger valves also make use of capillary pumps to ensure a continuous flow at a pre-determined flow rate. It should be noted that when the flow rate in the channel decreases, Reynolds numbers also decrease, resulting in inefficiency of the serpentine

mixer. Therefore, if this approach is taken, the herringbone structure would be more suited as mixing structure.

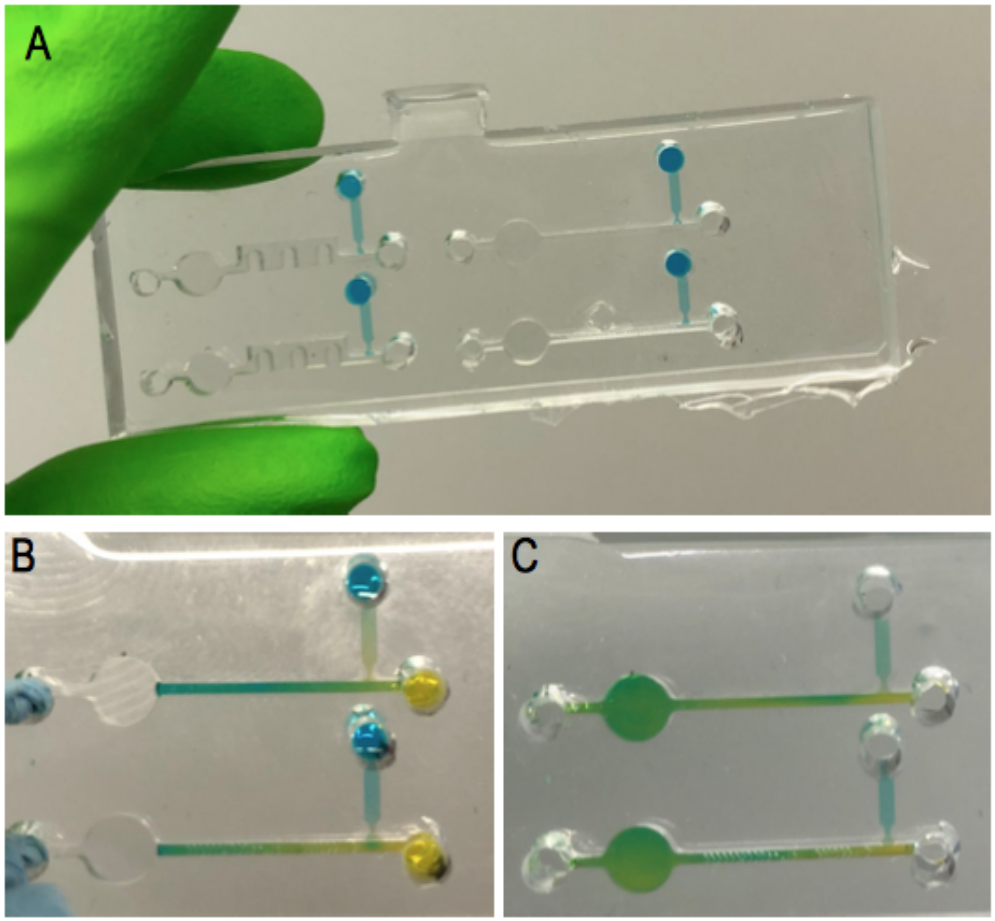

Figure 17: A) Narrow channel is filled with blue food dye via inlet B) After 10 minutes, yellow food dye is pipetted into the inlet of the deep channel C) The deep channel is completely filled.

9 Future Outlook

First steps have been taken for the development of a microfluidic device for POCT of free thiol levels in finger-prick blood. However, not all sample preparation steps are currently incorporated into the design and a plate-reader is still used for the read-out of the PDMS device. Therefore, more work needs to be done to obtain a fully POC device. In addition, further experiments need to be performed to validate and optimize the current design.

9.1 Current Design

The inter-CV of the absorbance measurements on-chip (path length = 3 mm) have been calculated using 6 PDMS devices, all with one background and one DTNB measurement. The UMCG normally utilizes a minimum of 10 separate assays for the determination of the precision. For the reservoirs with a path length of 2 mm, only 4 PDMS devices have been measured. Therefore, a larger scale experiment should be performed utilizing at least 10 separate PDMS devices to meet the validation requirements of the UMCG.

For the calculation of the free thiol levels using on-chip absorbance measurement, a calibration curve measured on the PDMS device is used. Due to the PDMS device only containing 2 usable reservoirs per path length (3 mm and 2 mm), several PDMS devices were used to fabricate this calibration curve. In the current protocol of the UMCG, on each individual wells plate a calibration curve is added for the free thiol level calculations. In our case, a calibration curve fabricated once using 8 PDMS devices is used for all further calculations. To test if this calibration curve is reproducible, multiple calibration curves should be measured on different days. To enable faster measurement of calibration curves, the current design could be adjusted to contain 7 usable reservoirs with consistent path length.

The calculation of free thiols at a path length of 2 mm gives a higher value when compared to measurements using a path length of 3 mm and the 384 wells plate. This could be due to an error in the calibration curve measurement. Further experiments should be performed using the 2 mm path length to see if this lower path length can be utilized, as it is beneficial to reduce the amount of sample required.

The serpentine mixer was not correctly fabricated with the micro mill, probably due to too small distances between the channels. The current design should be adjusted and fabricated, to be able to test the efficiency of the serpentine mixer. If a capillary pump is incorporated into the device with a low pre-set fluid velocity, the Reynolds number of the flow decreases as it becomes more laminar. In this case, the serpentine mixer would not be efficient and this approach can be discarded. The staggered herringbone mixer tested did not show a noticeable increase of mixing efficiency. Enlargement of the groove dimensions could possibly increase mixing efficiency, as this results in larger disruptions of the flow pattern.

The reservoir of the current design has a volume of 45.6 μL for a 3 mm path length and 30 μL for a 2 mm path length. As finger-prick blood will ultimately be used as sample, it is desirable to use a lower sample volume. The reservoir is designed to be slightly bigger than a well of a 384 wells plate, to correct for any alignment errors in the plate reader. The final microfluidic device will not be measured using a plate reader, but with a small read-out device. When this new read-out device is designed, a smaller read-out area would significantly reduce the amount of sample required to fill the reservoir. Another approach to lower the required sample volume is to miniaturize the microchannels connecting the inlets, the detection reservoir and the outlets. Experiments can be performed to study if the length, height and the width of the microchannels can be lowered without affecting the operation of the device.

In the current design, only one read-out reservoir for absorbance is present. For the detection of free thiol levels, both a background measurement and a measurement after the addition of DTNB are required. This shows that the design should be adjusted to incorporate 2 read-out areas for absorbance; one before and one after the addition of DTNB. This should also be taken into account when designing the read-out device.

9.2 On-chip Sample Preparation

To achieve a fully POC device, all sample preparation steps should be incorporated into the microfluidic device. The current inlet sample is diluted plasma, however to achieve a sample-in-answer-out device, the inlet sample should be whole finger-prick blood. The design of the device should be adjusted to incorporate plasma separation and dilution.

9.2.1 Plasma Dilution

For the incorporation of plasma dilution, the trigger valve and mixer component of the DTNB mixing step could be re-used. However, this requires the user to manually add both the DTNB, Tris buffer and finger-prick blood to the microfluidic device. This is not a difficult action, however you want a POC device to have the least possible manual steps, as they also increase the chance of wrong use and read-out of the device.

Reagent storage on-chip could reduce the amount of manual steps the user has to perform, in this approach reagents are integrated into the microfluidic device during fabrication. A variety of integration methods are used in literature, along with different approaches to release the pre-stored liquid. However, when a liquid is pre-stored, often actions are required to release the liquid. These actions can also be incorporated into the read-out device. For example, Chen et al. [74] pre-stores liquids (buffers) in flexible pouches on the chip surface. These pouches are ruptured by a linear motor with a plunger, releasing the liquid in a controlled manner. This release by rupture can also be manually performed by the user, e.g. using a sharp device such as a needle. Smith et al. [75] make use of blister pouches for reagent storage, again reagents can be released through manual (pressing with a finger) or automated compression leading to rupture of the pouches. It should be taken into account that pre-storage of liquids can increase the cost of the devices as it results in a more complex fabrication process. [76] Furthermore, the material of the blisters/pouches should be compatible with the liquid, to ensure a long shelf-life. [75]

9.2.2 Plasma Separation

In many microfluidic applications, plasma is the desired sample for biomarker measurements. The standard separation process is centrifugation, which is performed using bulky centrifuges in the laboratory. To enable on-chip plasma separation, multiple approaches have been explored in a great number of studies, including both active and passive separation methods. For POC, passive mechanisms are best suited, as they are easier to fabricate, user-friendly and do not require external equipment. Passive separation mechanisms rely on microchannel geometry and hydrodynamic forces.

It is important that the device ensures a short separation time, as long-time separation processes increase the risk of coagulation of the whole blood sample. [77] Furthermore, the plasma sample should have a high purity ($> 99\%$) after separation, as other components of the whole blood could interfere during absorbance measurements. High-throughput is also important, to ensure that the required plasma volume is obtained from the whole blood sample. Plasma constitutes 55% of the total blood volume, therefore an extraction of 55 μL plasma from 100 μL whole blood would be optimal.

Passive plasma separation techniques can be divided into two major categories; mechanisms which make use of micro-filtration and mechanisms which do not. Micro-filtration approaches are often categorized into 1) Weir-type filtration 2) Dead-end pillar filtration 3) Cross-flow filtration and 4) Membrane filtration. Micro-filtration approaches often require dilution of the whole blood before separation, as a high hematocrit leads to clogging of the structures. Of these approaches, micro-filtration is the most popular in POC devices due to the least clogging issues. [78] Liu et al. [79] and Gervais et al. [80] utilize a commercially available membrane for plasma separation; the Vivid^{TM} Plasma Separation membrane. [81] This is a patented highly asymmetric membrane; the cellular components are captured in larger pores whereas the plasma flows down into the smaller pores on the downstream side of the membrane. Their website promises a 80% plasma yield within 2 minutes. However, Liu et al. report a yield of 12 μL plasma from 100 μL whole blood within 10 minutes. Uniform contact between the membrane and the receiving matrix has to be ensured to obtain plasma delivery. The underlying material must have enough capillary force to retrieve the plasma from the membrane, Gervais et al. uses small microfluidic channels to create this capillary pressure.

Passive separation without filtration makes use of 1) Curved Channels 2) Sedimentation 3) Bifurcation Law or 4) Wettability control. Separation in curved channels is based on dean flow fractionation; particles suspended in a microfluidic flow are sorted by their size due to centrifugal forces. However, this approach is not suited for finger-prick volumes as larger channel dimensions are required and whole blood needs to be diluted before separation. Sedimentation approaches are based on gravity and density differences between plasma and blood cells. The biggest disadvantage of sedimentation is the low separation velocity, however when using small sample volumes (e.g. finger-prick blood), this is not a big issue. Sedimentation approaches can be combined with micro-filtration structures to increase purity. [77] Maria et al. [82] and Forchelet et al. [83] both

exploit sedimentation to obtain plasma separation from whole finger-prick blood samples, with a purification efficiency of 99%. The bifurcation law, the Zweifach-Fung effect, describes a situation in which blood flows through a bifurcating region; red blood cells will almost all flow into the higher flow rate channel. This difference in flow rate can be obtained with a difference in diameter. Yang et al. [84] makes use of a bifurcation region which separates whole blood at a yield of 15-25% with a purity of 100%. Wettability gradients can also be used to provide a velocity gradient in the blood flow, separating the plasma from the blood. However, compared to the other techniques, separation time is long when using wettability gradients. In addition, surface modification makes the fabrication process complex.

In conclusion, sedimentation (combined with micro-filtration) and the bifurcation effect are most suited for plasma separation in our POC device; they can deal with undiluted whole blood samples and high separation efficiencies are obtained without clogging of the separation structures. The commercially available Vivid Plasma Separation Membrane could also be interesting to incorporate into our device, if a structure can be incorporated into the design to wick the plasma from the membrane.

9.3 Read-out Device

Current absorbance measurements are performed using the chip holder and the plate reader. However, a plate-reader is a bulky device which is not suited for POCT. To enable a POC read-out of the microfluidic device, a device should be developed for the absorbance measurements. This read-out device should be user-friendly, portable and reusable. It should have a cut-out where the microfluidic chip can be easily inserted after which it is automatically aligned with the light source and detector.

Optical fibers could be used to perform absorbance measurements, however alignment can be an issue, as precise alignment is required to ensure optical coupling. Furthermore, light from optical fibers is highly divergent, therefore both fibers need to be very close to yield sufficient irradiance. Lenses can be used to overcome this challenge, however it could still remain a challenge to work over a distance of 3 mm. Another option would be the use of LEDs as a light source in combination with a light detector, examples of detectors are photodiodes, light dependent resistors and phototransistors. [85] Flores et al. [86] created a plastic structure for the optical read-out of microfluidic devices, consisting of LEDs aligned with a photo transistor. Gao et al. [87] fabricated a portable system for absorption photometry consisting of a LED and photodiode detector.

9.4 Sample collection

Multiple devices are commercially available for the collection of finger-prick blood. A finger stick/lancet is frequently used to punch a small hole in the skin of the finger. This blood can then directly be placed on the inlet of the microfluidic device. However, this can also be done using a blood collection device, ensuring efficient and drip-free blood transfer to the inlet. Sarstedt has designed the Minivette; a blood collection device especially designed for POC applications. After punching a small hole in the skin using a finger stick/lancet, the Minivette tip is placed on the hole (Fig 18-1) and the blood is collected by capillary action (Fig 18-2). After collection of the finger-prick blood, the piston of the device is used to dispense the blood sample into the inlet (Fig 18-3), enabling precise dispensing of small whole blood volumes. This device ensures hygienic and secure sample transfer, preventing spillage. Furthermore, the collection tube can be coated with anti-coagulant reagents such as heparin and EDTA. This can be beneficial when blood clotting occurs during plasma separation. The Minivette POCT is available in a range of 10-200 μL volumes. [88]

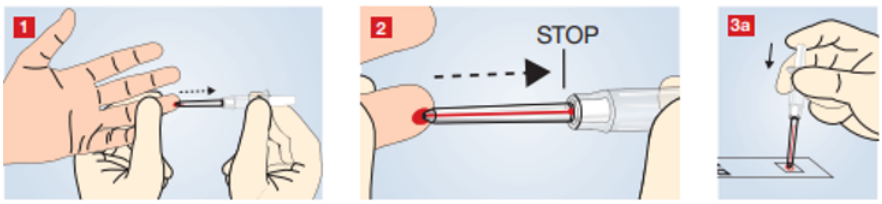

Figure 18: Use of Minivette for finger-prick blood collection. Reprinted from [88]

10 Conclusion

During this thesis, first steps were taken towards the design and fabrication of a microfluidic device for POCT of free thiol levels in plasma. The current protocol utilizing DTNB for free thiol detection was successfully adjusted to lower plasma volumes (6 μL). An inter-CV of 10.5% shows that this method has acceptable repeatability. Next, steps were taken to incorporate the last two steps of this protocol into a microfluidic device; mixing of diluted plasma with DTNB and absorbance measurements.

A chip holder and PDMS device were designed, allowing on-chip absorbance measurements. Experiments showed that on-chip absorbance measurements show lower variation when compared to similar measurements in a 384 wells plate. Trigger valves were designed and fabricated, the valves with a height difference of 1100 and 1500 μm had a success rate of 100%: liquid in the narrow channel was stopped for at least 10 minutes. A herringbone mixer structure was fabricated using micro milling of a master mould and PDMS replication. No noticeable effect on mixing efficiency was seen.

Further steps need to be taken to develop a POC device for free thiol detection in finger-prick blood. Currently, the inlet sample is diluted plasma, where this should be whole blood. Plasma separation and dilution need to be incorporated into the current design. Further research will mainly focus on the design of these two sample preparation steps, in addition to further optimization of the current design.

11 Acknowledgements

First of all, I would like to thank my daily supervisor Loes Segerink, who was always enthusiastic and very helpful. Also thanks to my other supervisor from the University of Twente; Wouter Olthuis. I would also like to thank Arno Bourgonje, Harry van Goor, Sanne Gordijn and Anneke Muller Kobold from the UMCG. Even though our meetings took place very early in the morning, they were always fun and full of enthusiasm and critical questions. Thanks for always replying to my emails with kind words and optimism. Furthermore, I would like to thank Marian Bulthuis for the elaborate explanation of the current detection protocol. I really enjoyed my visit to the UMCG, during which Marian showed me how she performed the protocol.

During my master thesis, I enjoyed the working environment at the BIOS Lab on a Chip group. Thanks to all the staff and other students for making it a fun time. Special thanks to Nienke van Dongen, Jeroen Vollenbroek and Daria Bugakova for their help with the plate reader and micro mill. Also to Paul ter Braak, for the lab introduction and my many practical questions.

References

[1] Pedro Tauler Riera, Maurizio Volterrani, Ferdinando Iellamo, Francesco Fallo, Andrea Ermolao, William J. Kraemer, Nicholas A. Ratamess, Avery Faigenbaum, Andrew Philp, and Keith Baar. Redox Status. *Encyclopedia of Exercise Medicine in Health and Disease*, pages 751–753, 2012.

[2] Meghri Katerji, Maria Filippova, and Penelope Duerksen-Hughes. Approaches and methods to measure oxidative stress in clinical samples: Research applications in the cancer field. *Oxidative Medicine and Cellular Longevity*, 2019, 2019.

[3] Jean Charles Preiser. Oxidative stress. *Journal of Parenteral and Enteral Nutrition*, 36(2):147–154, 3 2012.

[4] Michalis G. Nikolaidis and Athanasios Z. Jamurtas. Blood as a reactive species generator and redox status regulator during exercise. *Archives of Biochemistry and Biophysics*, 490(2):77–84, 10 2009.

[5] Shampa Chatterjee. Oxidative Stress, Inflammation, and Disease. *Oxidative Stress and Biomaterials*, pages 35–58, 1 2016.

[6] Emilie Dubois-deruy, Victoriane Peugnet, Annie Turkieh, and Florence Pinet. Oxidative Stress in Cardiovascular Diseases. *Antioxidants 2020, Vol. 9, Page 864*, 9(9):864, 9 2020.

[7] Tian Tian, Ziling Wang, and Jinhua Zhang. Pathomechanisms of Oxidative Stress in Inflammatory Bowel Disease and Potential Antioxidant Therapies. *Oxidative Medicine and Cellular Longevity*, 2017, 2017.

[8] Mirthe H. Schoots, Sanne J. Gordijn, Sicco A. Scherjon, Harry van Goor, and Jan Luuk Hillebrands. Oxidative stress in placental pathology. *Placenta*, 69:153–161, 9 2018.

[9] Jeroen Frijhoff, Paul G. Winyard, Neven Zarkovic, Sean S. Davies, Roland Stocker, David Cheng, Annie R. Knight, Emma Louise Taylor, Jeannette Oettrich, Tatjana Ruskovska, Ana Cipak Gasparovic, Antonio Cuadrado, Daniela Weber, Henrik Enghusen Poulsen, Tilman Grune, Harald H.H.W. Schmidt, and Pietro Ghezzi. Clinical Relevance of Biomarkers of Oxidative Stress. *Antioxidants & redox signaling*, 23(14):1144–1170, 11 2015.

[10] Resat. Apak and Esra. Capanoglu. Measurement of Antioxidant Activity and Capacity : Recent Trends and Applications. page 354, 2017.

[11] Arno R. Bourgonje, Martin Feelisch, Klaas Nico Faber, Andreas Pasch, Gerard Dijkstra, and Harry van Goor. Oxidative Stress and Redox-Modulating Therapeutics in Inflammatory Bowel Disease. *Trends in Molecular Medicine*, 26(11):1034–1046, 11 2020.

[12] T. R. Sutton, M. Minnion, F. Barbarino, G. Koster, B. O. Fernandez, A. F. Cumpstey, P. Wischmann, M. Madhani, M. P. Frenneaux, A. D. Postle, M. M. Cortese-Krott, and M. Feelisch. A robust and versatile mass spectrometry platform for comprehensive assessment of the thiol redox metabolome. *Redox biology*, 16:359–380, 6 2018.

[13] Lucía Turell, Rafael Radi, and Beatriz Alvarez. The thiol pool in human plasma: the central contribution of albumin to redox processes. *Free radical biology & medicine*, 65:244–253, 2013.

[14] Alessio Bocedi, Giada Cattani, Lorenzo Stella, Renato Massoud, and Giorgio Ricci. Thiol disulfide exchange reactions in human serum albumin: the apparent paradox of the redox transitions of Cys34. *FEBS Journal*, 285(17):3225–3237, 9 2018.

[15] Hasmik Grigoryan, He Li, Anthony T Iavarone, Evan R Williams, and Stephen M Rappaport. Cys34 Adducts of Reactive Oxygen Species in Human Serum Albumin. 2012.

[16] Arno R. Bourgonje, Ruben Y. Gabriëls, Martin H. De Borst, Marian L.C. Bulthuis, Klaas Nico Faber, Harry Van Goor, and Gerard Dijkstra. Serum Free Thiols Are Superior to Fecal Calprotectin in Reflecting Endoscopic Disease Activity in Inflammatory Bowel Disease. *Antioxidants 2019, Vol. 8, Page 351*, 8(9):351, 9 2019.

[17] Amaal E. Abdulle, Arno R. Bourgonje, Lyanne M. Kieneker, Anne M. Koning, S. La Bastide-Van Gemert, Marian L.C. Bulthuis, Gerard Dijkstra, Klaas Nico Faber, Robin P.F. Dullaart, Stephan J.L. Bakker, Reinold O.B. Gans, Ron T. Gansevoort, Douwe J. Mulder, Andreas Pasch, and Harry Van Goor. Serum free thiols predict cardiovascular events and all-cause mortality in the general population: A prospective cohort study. *BMC Medicine*, 18(1):1–12, 5 2020.

[18] Mirthe H. Schoots, Martin F. Bourgonje, Arno R. Bourgonje, Jelmer R. Prins, Eline G.M. van Hoorn, Amaal E. Abdulle, Anneke C. Muller Kobold, Martin van der Heide, Jan Luuk Hillebrands, Harry van Goor, and Sanne J. Gordijn. Oxidative stress biomarkers in fetal growth restriction with and without preeclampsia. *Placenta*, 115:87–96, 11 2021.

[19] Przemysław J. Włodek, Olgierd B. Smolenski, Grazyna Chwatko, Małgorzata B. Iciek, Andrzej Miłkowski, Edward Bald, and Lidia Włodek. Disruption of thiol homeostasis in plasma of terminal renal failure patients. *Clinica chimica acta; international journal of clinical chemistry*, 366(1-2):137–145, 4 2006.

[20] Emmelien E.M. Schillern, Andreas Pasch, Martin Feelisch, Femke Waanders, Steven H. Hendriks, Rik Mencke, Geert Harms, Klaas H. Groenier, Henk J.G. Bilo, Jan Luuk Hillebrands, Harry van Goor, and Peter R. van Dijk. Serum free thiols in type 2 diabetes mellitus: A prospective study. *Journal of clinical & translational endocrinology*, 16, 6 2019.

[21] Gethin J. McBean, Mutay Aslan, Helen R. Griffiths, and Rita C. Torrão. Thiol redox homeostasis in neurodegenerative disease. *Redox Biology*, 5:186, 8 2015.

[22] Mohammad H. Yarmohammadian, Fatemeh Rezaei, Abbas Haghshenas, and Nahid Tavakoli. Overcrowding in emergency departments: A review of strategies to decrease future challenges. *Journal of Research in Medical Sciences : The Official Journal of Isfahan University of Medical Sciences*, 22(1), 2017.

[23] Juhwan Park, Dong Hyun Han, and Je Kyun Park. Towards practical sample preparation in point-of-care testing: user-friendly microfluidic devices. *Lab on a Chip*, 20(7):1191–1203, 3 2020.

[24] Kleanthi Dima. Hot Topic in Laboratory Medicine-EuroLabNews n. 2/2021 Point of care testing (POCT) Present and Future.

[25] Behzad Nasseri, Neda Soleimani, Navid Rabiee, Alireza Kalbasi, Mahdi Karimi, and Michael R. Hamblin. Point-of-care microfluidic devices for pathogen detection. *Biosensors and Bioelectronics*, 117:112–128, 10 2018.

[26] Commercialization of microfluidic point-of-care diagnostic devices{, author = Chin, Curtis D and Linder, Vincent and Sia, Samuel K, url = www.rsc.org/loc, doi = 10.1039/c2lc21204h.

[27] ab-on-a-ch evices for linical Lab-on-a-chip devices for clinical diagnostics Measuring into a new dimension. 2013.

[28] Jing Wu and Min Gu. Microfluidic sensing: state of the art fabrication and detection techniques. *https://doi.org/10.1117/1.3607430*, 16(8):080901, 8 2011.

[29] Suzanne Smith, Dario Mager, Alexandra Perebikovsky, Ehsan Shamloo, David Kinahan, Rohit Mishra, Saraí M. Torres Delgado, Horacio Kido, Satadal Saha, Jens Ducrée, Marc Madou, Kevin Land, and Jan G. Korvink. CD-based microfluidics for primary care in extreme point-of-care settings. *Micromachines*, 7(2), 2016.

[30] Introduction to lab-on-a-chip 2020: review, history and future - Elveflow.

[31] Changqing Yi, Qi Zhang, Cheuk Wing Li, Jun Yang, Jianlong Zhao, and Mengsu Yang. Optical and electrochemical detection techniques for cell-based microfluidic systems. *Analytical and Bioanalytical Chemistry*, 384(6):1259–1268, 3 2006.

[32] Paul C White, Nathan S Lawrence, James Davis, and Richard G Compton. Electrochemical Determination of Thiols: A Perspective.

[33] Nathan S. Lawrence, James Davis, and Richard G. Compton. Electrochemical detection of thiols in biological media. *Talanta*, 53(5):1089–1094, 1 2001.

[34] Svetlana Gracheva, Callum Livingstone, and James Davis. Development of a disposable potentiometric sensor for the near patient testing of plasma thiol concentrations. *Analytical Chemistry*, 76(13):3833–3836, 7 2004.

[35] T. Inoue and J. R. Kirchhoff. Electrochemical detection of thiols with a coenzyme pyrroloquinoline quinone modified electrode. *Analytical Chemistry*, 72(23):5755–5760, 12 2000.

[36] Zeynep Aydogmus, Ahmad Sarakbi, and Jean Michel Kauffmann. Determination of Thiols and Free Thiol Content in a Protein with Liquid Chromatography Coupled to Amperometric Detection at a Silver Based Carbon Paste Electrode. *Electroanalysis*, 28(11):2703–2708, 11 2016.

[37] G-Biosciences. Ellman's Reagent 5,5'-dithio-bis-(2-nitrobenzoic acid) (DTNB) (Cat. # BC87).

[38] Sam Ang Supharoek, Napaporn Youngvises, and Jaroon Jakmunee. A simple microfluidic integrated with an optical sensor for micro flow injection colorimetric determination of glutathione. *Analytical sciences : the international journal of the Japan Society for Analytical Chemistry*, 28(7):651–656, 2012.

[39] Forough Ghasemi, M. Reza Hormozi-Nezhad, and Morteza Mahmoudi. A colorimetric sensor array for detection and discrimination of biothiols based on aggregation of gold nanoparticles. *Analytica Chimica Acta*, 882:58–67, 7 2015.

[40] Hu Xu, Yiwen Wang, Xiaomei Huang, Yan Li, Hua Zhang, and Xinhua Zhong. Hg2+-mediated aggregation of gold nanoparticles for colorimetric screening of biothiols. *Analyst*, 137(4):924–931, 1 2012.

[41] Stephanie Knowlton, Ashwini Joshi, Philip Syrrist, Ahmet F. Coskun, and Savas Tasoglu. 3D-printed smartphone-based point of care tool for fluorescence- and magnetophoresis-based cytometry. *Lab on a Chip*, 17(16):2839–2851, 8 2017.

[42] Jinyu Sun, Liangwei Zhang, Xiaolong Zhang, Yuesong Hu, Chunpo Ge, and Jianguo Fang. An ultrafast turn-on thiol probe for protein labeling and bioimaging. *Analyst*, 141(6):2009–2015, 3 2016.

[43] Bo Hu, Yang Zhao, Hai-Zhou Zhu, and Shu-Hong Yu. Selective Chromogenic Detection of Thiol-Containing Biomolecules Using Carbonaceous Nanospheres Loaded with Silver Nanoparticles as Carrier. 13:44, 2022.

[44] Info Note 804: UV-VIS Nomenclature and Units.

[45] Werner Mäntele and Erhan Deniz. UV–VIS absorption spectroscopy: Lambert-Beer reloaded. *Spectrochimica Acta Part A: Molecular and Biomolecular Spectroscopy*, 173:965–968, 2 2017.

[46] Greiner bio-one. Application Note - UV/VIS Spectroscopy in Microplates.

[47] Beer Lambert Law — Transmittance & Absorbance — Edinburgh Instruments.

[48] DTNB (Ellman's Reagent) (5,5-dithio-bis-(2-nitrobenzoic acid).

[49] Absorbance Measurements — BMG LABTECH.

[50] Seyed Mojtaba Moosavi and Sussan Ghassabian. Linearity of Calibration Curves for Analytical Methods: A Review of Criteria for Assessment of Method Reliability. *Calibration and Validation of Analytical Methods - A Sampling of Current Approaches*, 2 2018.

[51] St Louis. Gold Biotechnology Protocol Ellman's Test Protocol Quantitative Determination of Thiols.

[52] Paola Nieri, Sara Carpi, Stefano Fogli, Beatrice Polini, Maria Cristina Breschi, and Adriano Podestà. Cholinesterase-like organocatalysis by imidazole and imidazole-bearing molecules. *Scientific Reports*, 8, 4 2017.

[53] Sammerul U. Hassan, Aamira Tariq, Zobia Noreen, Ahmed Donia, Syed Z.J. Zaidi, Habib Bokhari, and Xunli Zhang. Capillary-Driven Flow Microfluidics Combined with Smartphone Detection: An Emerging Tool for Point-of-Care Diagnostics. *Diagnostics 2020, Vol. 10, Page 509*, 10(8):509, 7 2020.

[54] Ayokunle Olanrewaju, Maïwenn Beaugrand, Mohamed Yafia, and David Juncker. Capillary microfluidics in microchannels: from microfluidic networks to capillaric circuits. *Lab on a Chip*, 18(16):2323–2347, 8 2018.

[55] Shaoxi Wang, Xiafeng Zhang, Cong Ma, Sheng Yan, David Inglis, and Shilun Feng. A Review of Capillary Pressure Control Valves in Microfluidics. *Biosensors 2021, Vol. 11, Page 405*, 11(10):405, 10 2021.

[56] Melikhan Tanyeri and Savaş Tay. Viable cell culture in PDMS-based microfluidic devices. *Methods in Cell Biology*, 148:3–33, 1 2018.

[57] Say Hwa Tan, Nam Trung Nguyen, Yong Chin Chua, and Tae Goo Kang. Oxygen plasma treatment for reducing hydrophobicity of a sealed polydimethylsiloxane microchannel. *Biomicrofluidics*, 4(3), 2010.

[58] Roozbeh Safavieh and David Juncker. Capillarics: pre-programmed, self-powered microfluidic circuits built from capillary elements. *Lab on a Chip*, 13(21):4180–4189, 10 2013.

[59] Jerry M Chen Ae, Po-Chun Huang, and Mou-Gee Lin. Analysis and experiment of capillary valves for microfluidics on a rotating disk.

[60] A. O. Olanrewaju, A. Robillard, M. Dagher, and D. Juncker. Autonomous microfluidic capillaric circuits replicated from 3D-printed molds. *Lab on a Chip*, 16(19):3804–3814, 9 2016.

[61] Manda S. Williams, Kenneth J. Longmuir, and Paul Yager. A practical guide to the staggered herringbone mixer. *Lab on a chip*, 8(7):1121, 2008.

[62] Thomas H. Brown. Hydraulics. *Highway Engineering: Planning, Design, and Operations*, pages 641–695, 2016.

[63] Chia Yen Lee, Chin Lung Chang, Yao Nan Wang, and Lung Ming Fu. Microfluidic Mixing: A Review. *International Journal of Molecular Sciences 2011, Vol. 12, Pages 3263-3287*, 12(5):3263–3287, 5 2011.

[64] Kevin Ward and Z. Hugh Fan. Mixing in microfluidic devices and enhancement methods. *Journal of Micromechanics and Microengineering*, 25(9):094001, 8 2015.

[65] Lorenzo Capretto, Wei Cheng, Martyn Hill, and Xunli Zhang. Micromixing within microfluidic devices. *Topics in Current Chemistry*, 304:27–68, 2011.

[66] Huanhuan Shi, Kaixuan Nie, Bo Dong, Lemeng Chao, Fengxiao Gao, Mingyang Ma, Mengqiu Long, and Zhengchun Liu. Mixing enhancement via a serpentine micromixer for real-time activation of carboxyl. *Chemical Engineering Journal*, 392, 7 2020.

[67] Joshua Clark, Miron Kaufman, and Petru S. Fodor. Mixing Enhancement in Serpentine Micromixers with a Non-Rectangular Cross-Section. *Micromachines*, 9(3), 3 2018.

[68] Eszter L. Tóth, Eszter G. Holczer, Kristóf Iván, and Péter Fürjes. Optimized simulation and validation of particle advection in asymmetric staggered herringbone type micromixers. *Micromachines*, 6(1):136–150, 2015.

[69] Calculating Inter- and Intra-Assay Coefficients of Variability – Salimetrics.

[70] Alankar Shrivastava and VipinB Gupta. Methods for the determination of limit of detection and limit of quantitation of the analytical methods. *Chronicles of Young Scientists*, 2(1):21, 2011.

[71] Mathematics of simple regression.

[72] Capillary pumps for autonomous capillary systems{, year = 2006, author = Zimmermann, Martin and Schmid, Heinz and Hunziker, Patrick and Delamarche, Emmanuel, url = www.rsc.org/loc, doi = 10.1039/b609813d.

[73] Lei Zhang, Ben Jones, Bivragh Majeed, Yukari Nishiyama, Yasuaki Okumura, and Tim Stakenborg. Study on stair-step liquid triggered capillary valve for microfluidic systems. *Journal of Micromechanics and Microengineering*, 28(6), 3 2018.

[74] Dafeng Chen, Michael Mauk, Xianbo Qiu, Changchun Liu, Jitae Kim, Sudhir Ramprasad, Serge Ongagna, William R. Abrams, Daniel Malamud, Paul L.A.M. Corstjens, and Haim H. Bau. An integrated, self-contained microfluidic cassette for isolation, amplification, and detection of nucleic acids. *Biomedical Microdevices 2010 12:4*, 12(4):705–719, 4 2010.

[75] Suzanne Smith, René Sewart, Holger Becker, Pieter Roux, and Kevin Land. Blister pouches for effective reagent storage on microfluidic chips for blood cell counting. *Microfluidics and Nanofluidics*, 20(12), 12 2016.

[76] D. Mark, S. Haeberle, G. Roth, F. Von Stetten, and R. Zengerle. Microfluidic lab-on-a-chip platforms: Requirements, characteristics and applications. *NATO Science for Peace and Security Series A: Chemistry and Biology*, pages 305–376, 2010.

[77] Yudong Wang, Bharath Babu Nunna, Niladri Talukder, Ernst Emmanuel Etienne, and Eon Soo Lee. Blood Plasma Self-Separation Technologies during the Self-Driven Flow in Microfluidic Platforms. *Bioengineering (Basel, Switzerland)*, 8(7), 7 2021.

[78] Hong Miao Ji, Victor Samper, Yu Chen, Chew Kiat Heng, Tit Meng Lim, and Levent Yobas. Silicon-based microfilters for whole blood cell separation. *Biomedical Microdevices 2007 10:2*, 10(2):251–257, 10 2007.

[79] Changchun Liu, Michael Mauk, Robert Gross, Frederic D. Bushman, Paul H. Edelstein, Ronald G. Collman, and Haim H. Bau. Membrane-based, sedimentation-assisted plasma separator for point-of-care applications. *Analytical Chemistry*, 85(21):10463–10470, 11 2013.

[80] Luc Gervais and Emmanuel Delamarche. Toward one-step point-of-care immunodiagnostics using capillary-driven microfluidics and PDMS substrates. *Lab on a Chip*, 9(23):3330–3337, 12 2009.

[81] Vivid™ Plasma Separation Membrane - Medical Blog — Pall Corporation.

[82] M. Sneha Maria, P. E. Rakesh, T. S. Chandra, and A. K. Sen. Capillary flow-driven microfluidic device with wettability gradient and sedimentation effects for blood plasma separation. *Scientific Reports*, 7, 3 2017.

[83] D. Forchelet, S. Béguin, T. Sajic, N. Bararpour, Z. Pataky, M. Frias, S. Grabherr, M. Augsburger, Y. Liu, M. Charnley, J. Déglon, R. Aebersold, A. Thomas, and P. Renaud. Separation of blood microsamples by exploiting sedimentation at the microscale. *Scientific Reports 2018 8:1*, 8(1):1–9, 9 2018.

[84] Sung Yang, Akif Ündar, and Jeffrey D. Zahn. A microfluidic device for continuous, real time blood plasma separation. *Lab on a Chip*, 6(7):871–880, 6 2006.

[85] Bambang Kuswandi, Nuriman, Jurriaan Huskens, and Willem Verboom. Optical sensing systems for microfluidic devices: A review. *Analytica Chimica Acta*, 601(2):141–155, 10 2007.

[86] G. Flores, F. Perdigones, C. Aracil, M. Cabello, and J. M. Quero. Microfluidic platform with absorbance sensor for glucose detection. *Proceedings of the 2015 10th Spanish Conference on Electron Devices, CDE 2015*, 4 2015.

[87] Rongke Gao, Yuanmeng Wu, Jing Huang, Le Song, Haiyang Qian, Xuefei Song, Lei Cheng, Rui Wang, Lin bao Luo, Gang Zhao, and Liandong Yu. Development of a portable and sensitive blood serum test system using LED-based absorption photometry and pump-free microfluidic technology. *Sensors and Actuators B: Chemical*, 286:86–93, 5 2019.

[88] Minivette POCT - Sarstedt.

Appendix

A Abstract Submitted to Redox Conference

DESIGN OF A MICROFLUIDIC DEVICE FOR POINT-OF-CARE TESTING OF FREE THIOL LEVELS IN PLASMA

HAMMINK, Esmay, VAN GOOR, Harry, BOURGONJE, Arno, MULLER KOBOLD, Anneke, GORDIJN, Sanne, SEGERINK, Loes

Introduction: Plasma free thiol levels reliably reflect the redox status, as the sulfhydryl group (R-SH) is readily oxidized by oxidants. Studies have shown the potential of plasma free thiol levels as biomarker in various conditions, such as inflammatory bowel disease1. Current detection of free thiols is time-consuming and laborious. Here we developed a microfluidic device for point-of-care detection of free thiols using finger-prick blood.
Materials & Methods: The standard protocol for free thiol detection with DTNB described by Ellman was adjusted and applied to lower volume samples. A PMMA master mold was fabricated using micro milling for the replication of PDMS microfluidic devices, on which absorbance measurements were performed.
Results: Free thiol measurements on 6 μL of plasma resulted in an inter-CV <5% and an intra-CV <11% (n=8). On-chip absorbance measurements resulted in an intra-CV <4% (n=6), determined concentrations were comparable to the values obtained with the current method (average factor of 1.03).
Conclusion: Our results show the promising potential of microfluidic devices for the rapid determination of free thiol levels in small volume plasma samples. To achieve point-of-care testing, further sample preparation steps need to be integrated on the microfluidic device; mixing, plasma separation and dilution.

B Protocol UMCG; colorimetric detection of free thiol groups

Specifications of reagents used:

Chemicals	CAS-Nummer	Sigma Aldrich
L-Cystein	77-86-1	Merck
Tris	77-86-1	Merck
EDTA	60-00-4	Serva
DTNB	69-78-3	Sigma Aldrich
K2HPO4	7758-11-04	Merck
KH2PO4	7778-77-0	Merck

The protocol for the detection of free thiol groups as currently used at the UMCG:

1. Spin plasma samples (10 min at 10 rcf), dilute 1:4 with 0.1 M Tris buffer (pH 8.2) (Merck)
2. Prepare fresh 10 mM L-Cystein to make calibration curve. For plasma: 15.625 to 1000 μM final concentration.
3. Add 90 μL diluted sample or standard in triplicates to flat bottom 96 well plate (Costar)
4. Measure background absorption at 412 nm, reference 630 nm
5. Add 20 μL 1.9 mM DTNB in phosphate buffer (0.1 M, pH 7)
6. Incubate 20 minutes at room temperature, in the dark.
7. Measure absorption at 412 nm, reference 630 nm
8. Determine concentration of samples using the L-Cystein standard solution.

C Adjusted Protocol Lower Sample Volume

The protocol for the detection of free thiol groups, adjusted to lower sample volumes:

1. Spin plasma samples (10 min at 10 rcf), dilute 1:4 with 0.1 M Tris buffer (pH 8.2) (Merck)
2. Prepare fresh 10 mM L-Cystein to make calibration curve. For plasma: 15.625 to 1000 μM final concentration.
3. Add 16, 24 and 40 μL diluted sample or standard in triplicates to flat bottom 96 well plate (Costar)
4. Measure background absorption at 412 nm, reference 630 nm
5. Add 3.5 μL, 5.3 μL and 8.9 μL 1.9 mM DTNB in phosphate buffer (0.1 M, pH 7) respectively to the 16, 24 and 40 μL samples.
6. Incubate 20 minutes at room temperature, in the dark.
7. Measure absorption at 412 nm, reference 630 nm
8. Determine concentration of samples using the L-Cystein standard solution.

D Chip Holder

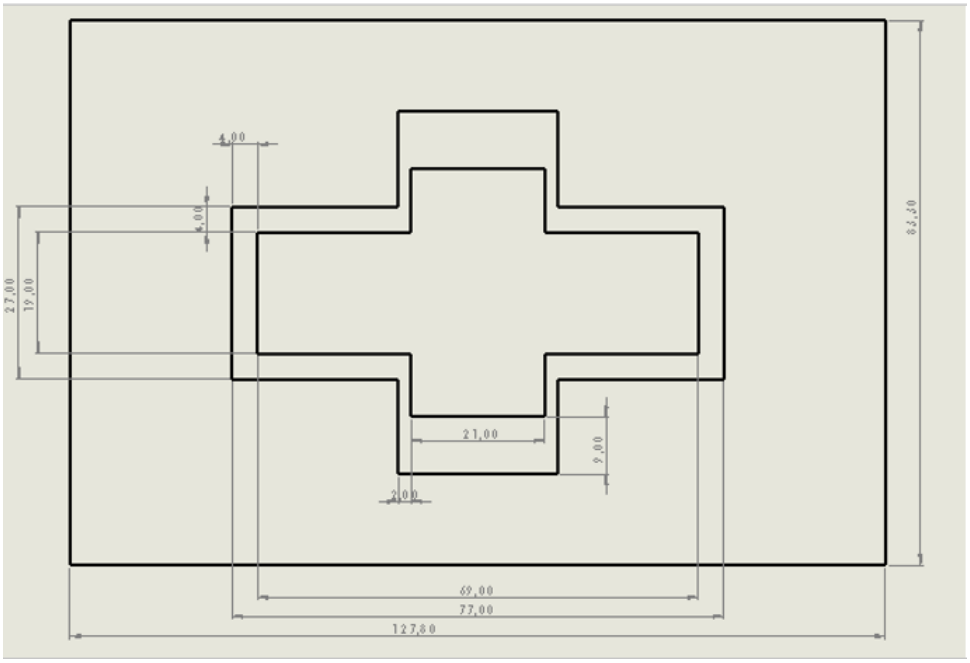

Figure D.1: Drawing of chip holder, top view

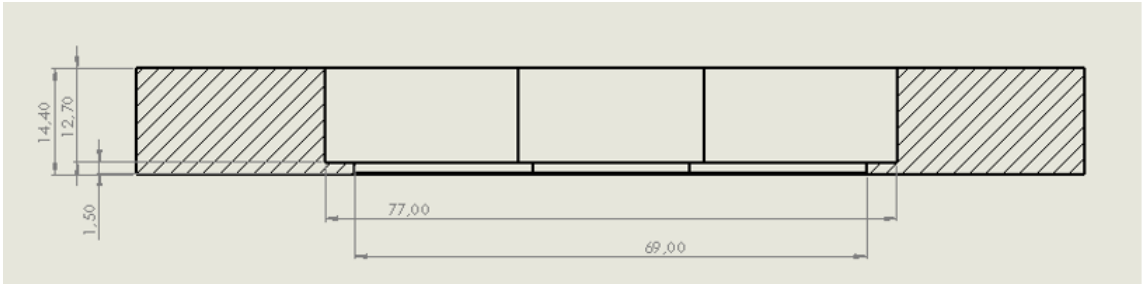

Figure D.2: Drawing of chip holder, side view

E Initial Design On-chip Absorbance

Initial design of positive mould for microfluidic device fabrication consisted of an inlet, channel and reservoir for absorbance measurements. The shape of the 384 wells can be best described as an inverted truncated pyramid. However, the reservoir of this microfluidic device is designed cuboidal, due to easier fabrication. The dimensions of the reservoir are 3.45 mm x 3.45 mm, as this is the width of the microwell at the height of 3.06 mm. This is calculated with the formula for a truncated pyramid:

$$V = \frac{1}{3} * h * (a^2 + b^2 + ab)$$

Where V is the volume (mm^3), h is the height (μm), a is the side length of the small base and b is the side length of the large base (μm). The channel has a length of 4 mm, height of 1 mm and a width of 700 μm. The inlet has a diameter of 1.5 mm.

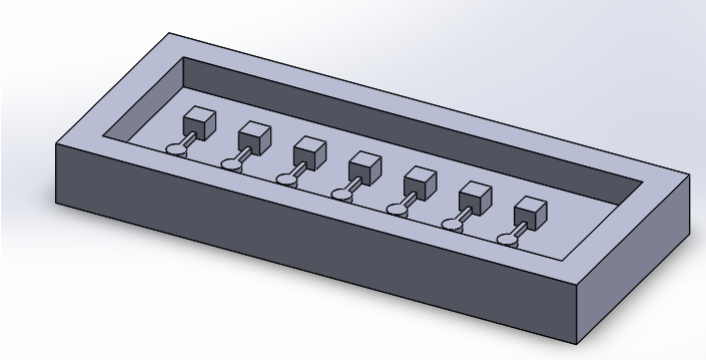

Figure E.1: 3D View of Initial Design of Chip

Filling of the reservoirs was only possible when an air outlet was punched close to the reservoir. Still, filling of the reservoir resulted in the presence of air bubbles in the reservoir, affecting the absorbance measurements. Furthermore, the inlet diameter of 1.5 mm is too big for a micro pipette tip. Based on these findings, the following adjustments were made to the design:

- Inlet diameter is decreased to 0.75 mm.
- Various channel heights are incorporated in the design, to study the effect of the channel height on bubble formation.
- Cuboid reservoirs are transformed to cylindrical reservoirs.
- An outlet is added to the design.
- Reservoirs with a height of 2 mm are added, to see if reduction of path length is feasible.

F Trigger Valves

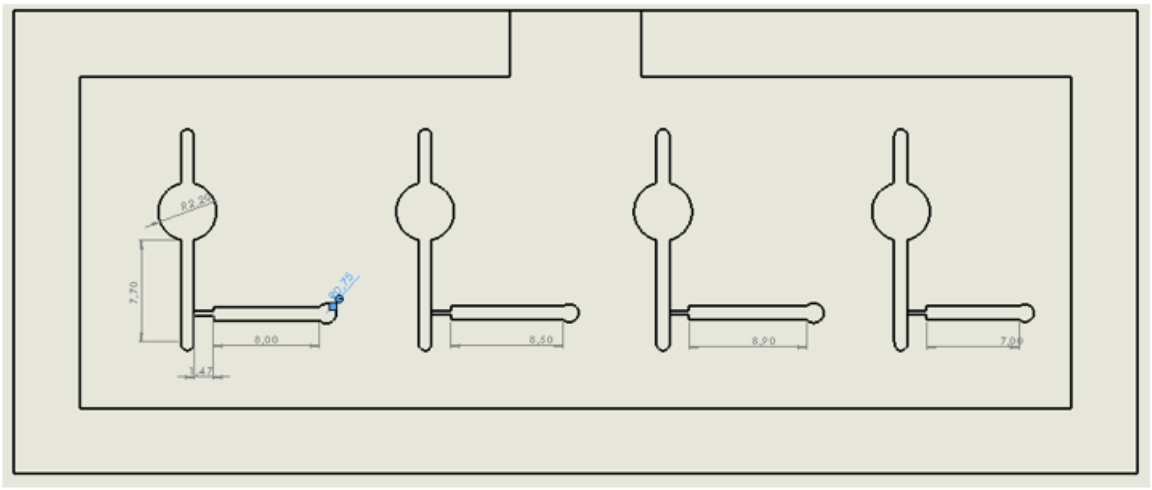

Figure F.1: Drawing in SolidWorks of Master Mould containing trigger valve structures

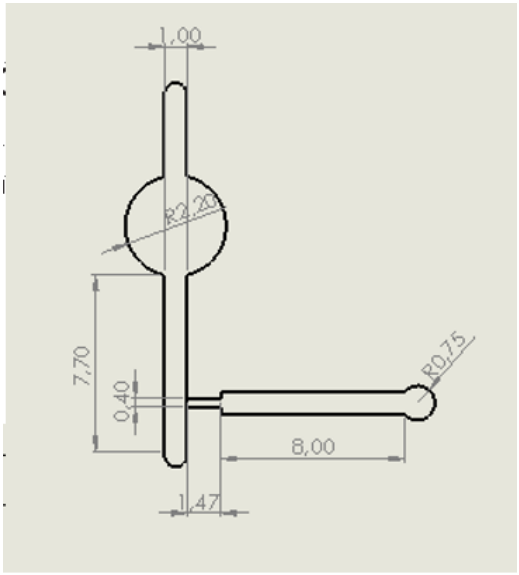

Figure F.2: Drawing in SolidWorks of Zoom-in on Master Mould containing trigger valve structures

G Microfluidic Mixer

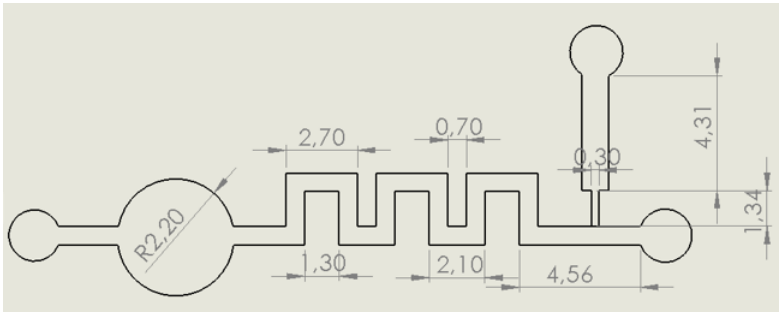

Figure G.1: Drawing in SolidWorks of Serpentine Mixer

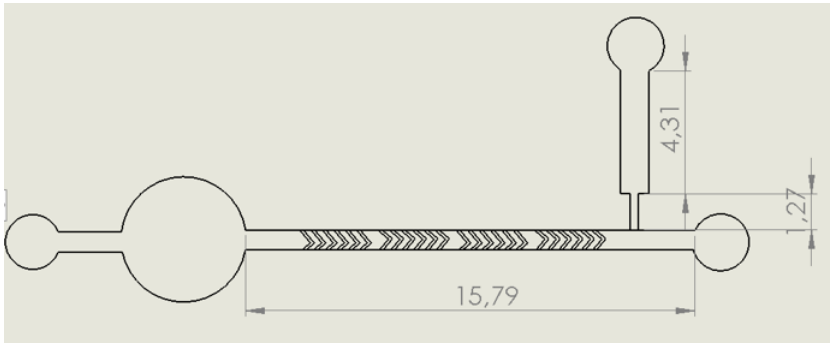

Figure G.2: Drawing in SolidWorks of Staggered Herringbone Mixer

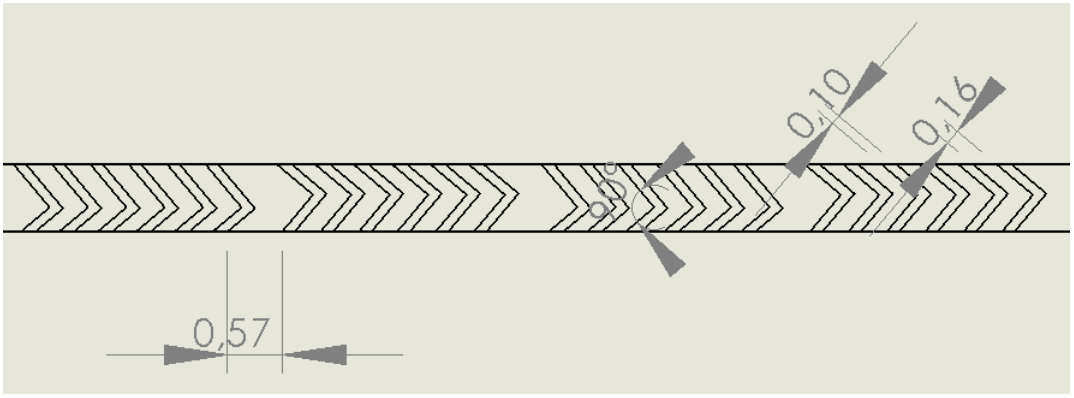

Figure G.3: Drawing in SolidWorks of Staggered Herringbone Mixer, zoomed in on herringbone grooves

H Experiments PBS Spiked with L-cysteine

Table H.1: Overall results for the determination of free thiol levels in 4 μL of PBS spiked with 1 mM L-cysteine, 1:4 diluted in 0.1 M Tris buffer (pH 8.2) to 16 μL, showing average concentration (μM), standard deviation (SD), intra-coefficient of variation (CV) and single values (μM).

Sample name	Concentration (μM)	SD (μM)	CV (%)	Single values (μM)		
0	16.2	15.2	93.8	19.4	32.9	-3.8
15.625	21.8	0.2	1.0	22.1	21.6	22.7
31.25	59.0	1.7	3.0	56.5	59.8	60.5
62.5	66.8	2.7	4.0	66.0	64.0	70.4
125	126.7	1.7	1.4	128.8	126.8	124.6
250	248.6	8.4	3.4	252.1	237.1	256.7
500	515.7	11.4	2.2	531.6	510.1	505.3
1000	1068.4	27.3	2.6	1059.1	1105.5	1040.6

Table H.2: Overall results for the determination of free thiol levels in 6 μL of PBS spiked with 1 mM L-Cystein, 1:4 diluted in 0.1 M Tris buffer (pH 8.2) to 24 μL, showing average concentration (μM), standard deviation (SD), intra-coefficient of variation (CV) and single values (μM).

Sample name	Concentration (μM)	SD (μM)	CV (%)	Single values (μM)		
0	24.2	1.9	7.6	21.6	25.8	25.2
15.625	27.3	0.8	2.9	26.5	28.1	27.0
31.25	65.4	2.3	3.4	62.9	65.0	68.3
62.5	73.8	2.5	3.4	75.4	70.2	75.7
125	130.1	1.9	1.5	132.1	130.6	127.5
250	245.5	2.2	0.9	248.0	246.0	242.7
500	492.4	14.4	2.9	512.7	483.0	481.6
1000	998.4	17.6	1.8	990.8	1022.7	981.7

Table H.3: Overall results for the determination of free thiol levels in 10 μL of PBS spiked with 1 mM L-Cystein, 1:4 diluted in 0.1 M Tris buffer (pH 8.2) to 40 μL, showing average concentration (μM), standard deviation (SD), intra-coefficient of variation (CV) and single values (μM).

Sample name	Concentration (μM)	SD (μM)	CV (%)	Single values (μM)		
0	11.5	1.1	9.8	12.8	11.8	10.0
15.625	13.6	2.9	21.0	10.8	16.5	15.0
31.25	56.6	3.5	6.2	61.2	52.8	55.8
62.5	62.1	1.6	2.6	64.2	61.9	60.3
125	124.5	2.6	2.1	127.8	124.3	121.5
250	252.6	6.2	2.4	261.4	248.1	248.4
500	509.2	5.6	1.1	517.1	504.5	506.0
1000	1037.1	21.8	2.1	1058.2	1045.9	1007.0

I Experiments Low Volumes Plasma

Table I.1: Concentration (μM), standard deviation (SD), coefficient of variation (CV) and single values of free thiol detection in 4 μL of plasma.

Sample name	Concentration (μM)	SD (μM)	CV (%)	Single Values (μM)		
1	363.8	27.3	7.5	341.5	366.0	383.7
2	354.4	4.6	1.3	349.7	359.0	412.6
3	349.9	29.9	8.6	391.8	333.8	324.0
4	336.3	14.4	4.3	341.6	350.8	316.6

Table I.2: Concentration (μM), standard deviation (SD), coefficient of variation (CV) and single values of free thiol detection in 6 μL of plasma.

Sample name	Concentration (μM)	SD (μM)	CV (%)	Single Values (μM)		
1	363.8	27.3	7.5	341.5	366.0	383.7
2	354.5	4.6	1.3	349.7	358.0	412.6
3	349.9	29.9	8.6	391.8	333.8	324.0
4	336.3	14.4	4.3	341.6	350.8	316.6

Table I.3: Concentration (μM), standard deviation (SD), coefficient of variation (CV) and single values of free thiol detection in 10 μL of plasma.

Sample name	Concentration (μM)	SD (μM)	CV (%)	Single Values (μM)		
1	269.1	42.6	15.8	211.3	312.7	283.2
2	286.5	34.9	12.2	251.7	312.4	312.6

J Colorimetric Detection

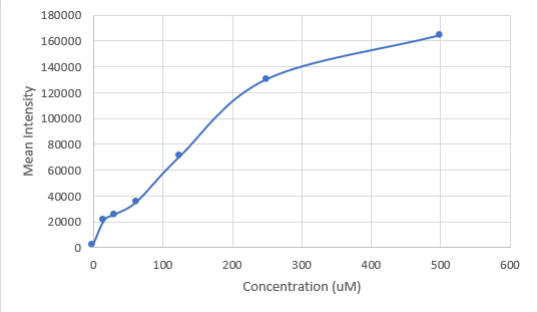

Figure J.1: Mean intensity measured using imageJ, plotted against the detected free thiol concentration (μM) for a calibration curve of serially diluted 1 mM L-cystein in 0.1 M Tris (pH 8.2)

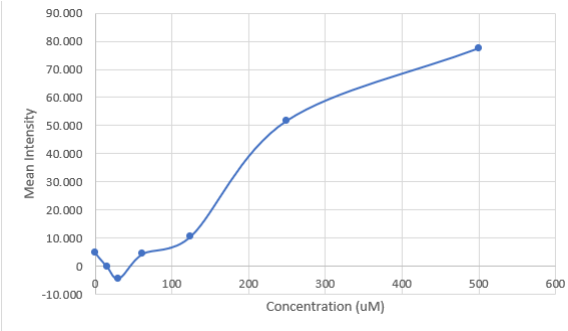

Figure J.2: Mean intensity measured using imageJ, plotted against the detected free thiol concentration (μM) for a 1:4 diluted calibration curve of serially diluted 1 mM L-cystein in 0.1 M Tris (pH 8.2)

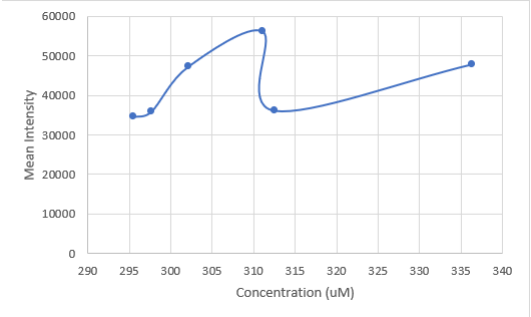

Figure J.3: Mean intensity measured using imageJ, plotted against the detected free thiol concentration (μM) for 1:4 diluted plasma samples

K Plasma Experiments On-chip

Table K.1: Free thiol concentrations (μM) measured in the 3 mm reservoir of the PDMS device, with calculated average concentration (μM), standard deviation (SD) and coefficient of variation (CV).

Sample name	Concentration (μM)
1	391.9
2	407.1
3	417.3
4	403.0
5	411.1
6	407.0
Av. Concentration (μM)	406.2
SD (μM)	7.8
CV (%)	1.9

Table K.2: Free thiol concentrations (μM) measured in the 2 mm reservoir of the PDMS device, with calculated average concentration (μM), standard deviation (SD) and coefficient of variation (CV).

Sample name	Concentration (μM)
1	464.7
2	446.9
3	413.2
4	443.0
Av. Concentration (μM)	441.9
SD (μM)	18.5
CV (%)	4.2

Table K.3: Free thiol concentrations (μM) measured in the 384 wells plate, with calculated average concentration (μM), standard deviation (SD) and coefficient of variation (CV).

Sample name	Concentration (μM)
1	384.9
2	358.3
3	394.4
4	415.2
5	430.0
Av. Concentration (μM)	396.5
SD (μM)	24.7
CV (%)	6.2